

Emotional Speech-driven 3D Body Animation via Disentangled Latent Diffusion

Kiran Chhatre¹ Radek Daněček² Nikos Athanasiou²

Giorgio Becherini² Christopher Peters¹ Michael J. Black² Timo Bolkart^{2*}

¹KTH Royal Institute of Technology, Sweden ²Max Planck Institute for Intelligent Systems, Germany

Abstract

Existing methods for synthesizing 3D human gestures from speech have shown promising results, but they do not explicitly model the impact of emotions on the generated gestures. Instead, these methods directly output animations from speech without control over the expressed emotion. To address this limitation, we present AMUSE, an emotional speech-driven body animation model based on latent diffusion. Our observation is that content (i.e., gestures related to speech rhythm and word utterances), emotion, and personal style are separable. To account for this, AMUSE maps the driving audio to three disentangled latent vectors: one for content, one for emotion, and one for personal style. A latent diffusion model, trained to generate gesture motion sequences, is then conditioned on these latent vectors. Once trained, AMUSE synthesizes 3D human gestures directly from speech with control over the expressed emotions and style by combining the content from the driving speech with the emotion and style of another speech sequence. Randomly sampling the noise of the diffusion model further generates variations of the gesture with the same emotional expressivity. Qualitative, quantitative, and perceptual evaluations demonstrate that AMUSE outputs realistic gesture sequences. Compared to the state of the art, the generated gestures are better synchronized with the speech content, and better represent the emotion expressed by the input speech. Our code is available at amuse.is.tue.mpg.de.

1. Introduction

Animating 3D bodies from speech has a wide range of applications, such as telepresence in AR/VR, avatar animation in games and movies, and to embody interactive digital assistants. While methods for speech-driven 3D body animation have recently shown great progress [5, 7, 34, 59, 107], existing methods do not adequately address one crucial factor: the impact of emotion from the driving speech signal on the generated gestures. Emotions and their expressions play

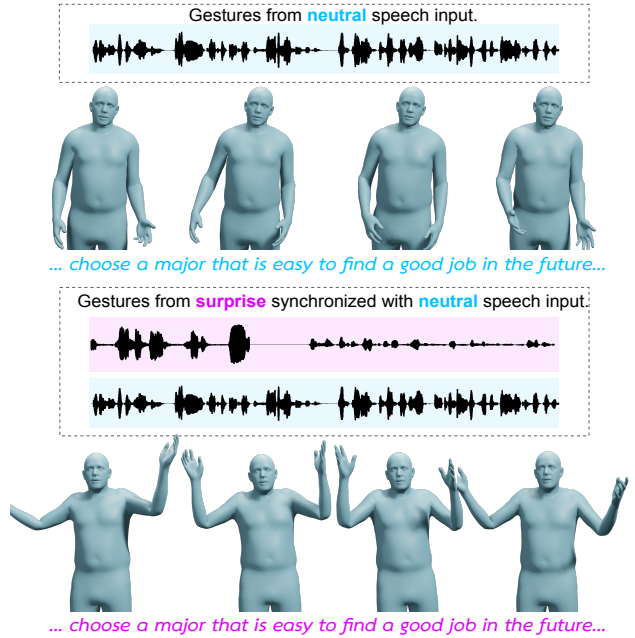


Figure 1. **Goal.** AMUSE generates realistic emotional 3D body gestures directly from a speech sequence (top). It provides user control over the generated emotion by combining the driving speech sequence with a different emotional audio (bottom).

a fundamental role in human communication [32, 38, 68] and have become an important consideration when designing computer systems that interact with humans in a natural manner [82, 83]. They are of central concern when synthesizing human animations for a wide variety of application contexts, such as Socially Interactive Agents [64]. Because of this, speech-driven animation systems must not only align movement with the rhythm of the speech, but should also be capable of generating gestures that are perceived as expressing the suitable emotion.

Many factors contribute to the perception of emotion and personal idiosyncrasies, such as facial expressions [19], gaze and eye contact [45], physiological responses [50], tone of voice [92], body language [69], and gestures [42]. When it comes to 3D animation, the most relevant factors

*Now at Google.

are facial expressions, gestures, and body language [101]. While emotional speech-driven animation methods have recently been proposed for 3D faces [18, 78, 95, 113], animating emotional bodies from speech remains under-explored.

Generating gestures solely from speech with emotional control is a difficult task. First, the mapping from audio to body motion is a non-deterministic many-to-many mapping, which is difficult to model. Gestures across subjects can vary when uttering the same sentence, and a single individual’s motions can change significantly across repetitions. Second, factoring out the impact of emotional state on the body motion from other, unknown factors, is difficult. This requires disentangling the effects of three different factors on the generated motion, namely content-based (i.e., gestures related to speech rhythm and word utterances), emotion-based, and those based on personal style. AMUSE addresses this by separating a speech sequence into content, emotion, and style latent vectors, which are then used to condition a latent diffusion model. Specifically, AMUSE consists of three main components: (1) an audio autoencoder trained to produce disentangled vectors of content, emotion, and style, (2) a 3D body motion prior in the form of a temporal variational autoencoder (VAE) to generate smooth and realistic gestures, and (3) a latent diffusion model, which generates 3D body motion given the input content, emotion, and style latent vectors.

Training such a model requires a speech-to-3D body dataset of sufficient scale, which is rich and diverse in speakers and emotions. BEAT [58] is a good candidate because it provides a large set of 3D gestures associated with single-person monologues. Unfortunately, the bodies are represented as skeletons, and it lacks face mocap markers and FLAME expressions. Instead, to produce realistic body animations, we require articulated 3D body surfaces. To overcome this, we convert BEAT sequences to SMPL-X [77] format using MoSh++ [65] and use the SMPL-X parameters for training. See [59] for comparison.

Our contributions are: (1) We present a framework to synthesize emotional 3D body gestures directly from speech. (2) We factor an input audio into disentangled content, emotion and style vectors, which enables us to separately control emotion in generated gestures. (3) We adapt temporal latent diffusion for multiple target conditions.

2. Related Work

2.1. 3D Conditional Human Motion Generation

Early works focus mostly on predicting [10, 16, 36, 44, 60, 67, 73, 91, 112, 115] or generating human motion [33, 52], but do not consider multi-modal control. Recently, conditional motion generation through other modalities, such as text [2, 8, 9, 17, 22, 30, 81], music [53, 71, 99], speech [35], or action labels [29, 79], has gained more attention. Be-

low, we focus on speech-driven motion generation methods, since they are the most relevant to our work.

2.2. Gesture Generation from Speech

Rule-based gesture synthesis. Embodied conversational agents (ECA) are designed to interact and communicate with humans. Using the Behavior Markup Language (BML) [47] one can build rule-based systems for humanoids based on predefined behaviors [84]. This is used for completion of a storytelling task in an expressive manner [48]. The BEAT rule-based toolkit [14] enables adding non-verbal behavior on top of a pre-animated figure. Thiebaut et al. [97] develop an ECA by using procedural animation techniques and keyframe interpolation. Marsella et al. [66] design a generalized rule-based agent to generate expressions, eye gaze, and gestures from speech. Each of these approaches are based on non-trainable, rule-based techniques that may require substantial manual modelling effort to adapt to new tasks.

Data-driven gesture synthesis. More recently, data-driven methods have superseded rule-based systems. Yoon et al. [110] use a fusion of text, audio and upper body gestures to learn an upper body gesture avatar, but can only control the style of individual speakers by sampling from their latent space. SpeechGestureMatching [35] generates 3D facial meshes and 3D keypoints of the body and hands from speech, but the outputs are separated and the method does not provide control over the generations. QPGesture [104] uses phase to better align the generated 3D skeleton-based gesturing avatars with the audio input. Ginosar et al. [23] and Diverse-3D-Hand-Gesture-Prediction [86] generate hand and arm motions only. Audio2Gestures [51] encode motion and audio to a low-dimensional latent space and generate gestures. SEEG [56] aims to generate gestures that align well with the semantics of the speech. DiffTTS [70] regresses speech and gestures at the same time, joining the two modalities in a single system. DiffGAN [3] retargets gestures across speakers in a low-resource setting. The GENE challenge [111] tackles gesticulation from speech alone using the Talking-with-Hands dataset [49]. Gesture2Vec [105] uses a machine translation model to translate text into gesture chunks and output full sequences using such quantized representations. TalkSHOW [107] uses a VQ-VAE to generate 3D human bodies gesturing with facial expressions from speech segments, but in an uncontrolled manner. Similarly, Co-speech gesture [63] uses an RQ-VAE to generate different gestures from speech. Alternative gesture generation from speech methods have been proposed such as reinforcement learning [96], self-supervised pre-training [43], and diffusion [70, 116]. BodyFormer [75] introduces a dataset of pseudo-groundtruth and a transformer-based method for generating gestures from speech. However, none of these methods provide explicit

emotional control over the generated motion.

For controllable generation, GestureDiffuCLIP [7] incorporates multiple conditions including CLIP [87] text features, video, or motion prompts via AdaIn [40] layers to generate gestures from speech, however, it does not allow explicit control over the emotion conveyed by the driving audio. ListenDenoiseAction [5] combines conformers and the DiffWave [46] architecture to generate gestures that can be controlled by a style vector, RhythmicGesticulator [6] disentangles the latent space into a vector related to the semantics of the gesture and one related to the subtle variations, while DisCo [57] models content and rhythm. StyleGestures [4] adapts MoGlow [37], demonstrating limited control over some motion attributes like the speed and expressiveness of gestures. DiffuseStyleGesture [103] uses diffusion to generate diverse gestures from speech.

2.3. Emotion Control

Emotion classification and control has been little studied in 3D human motion generation with only a few methods using skeletal motion in multi-class classification. Ghaleb et al. [20] employ a spatio-temporal graph convolution network to classify gestures into four classes: preparation, stroke, retraction, and neutral. Li et al. [55], on the other hand, use hidden Markov models for emotion classification of human movement mocap data. Karras et al. [41] learn face animations of a single actor, and test their method on different tasks by modifying the latent vectors. However, there is no disentanglement mechanism, and they do not model the synchronization of the emotion with the with the facial motions. Recently, EmoTalk [78], animates emotional 3D faces from speech input with control over the emotion intensity and EMOTE [18] disentangles emotion and speech to allow emotion editing at test time. However, models solely intended for facial tasks like lip syncing and capturing expressions might not smoothly adapt to the complexity of whole-body movements and distinct articulation. Regarding emotion-conditioned motion generation, Aberman et al. [1] show style-transfer from video data to motion and provide some style-based control, but do not address speech-driven emotional gestures. Similarly, the ZeroEGGs [21] dataset contains some emotional gesture controls but also includes more generic styles of motion. The method requires the input of arbitrary frames of desired motion to encode a style, thereby relying on motions and speech as conditions during inference. Text-driven emotional gesticulation, as explored by Bhattacharya et al. [11, 12], emphasizes the generation of gestures based on textual cues, incorporating additional conditions such as speech, speaker ID, seed poses, as well as valence, arousal, and dominance triplets. However, these approaches do not provide the means to distill explicit emotion features, limiting free control over the generated gestures. Closer to

our work, EMoG [108] incorporates emotion cues from the BEAT dataset [58] to generate improved gesture quality without explicit emotion control. EmotionGesture [85] uses a TED Emotion Dataset and BEAT to incorporate emotion features in gesture generation and generate emotional gestures. Although they can generate emotional gestures, their method is not end-to-end and has no explicit motion control. Specifically, it uses an emotion-conditioned VAE after training to acquire diverse emotion features that are used to generate gestures without guarantees and control over emotion types. Wu et al. [102] introduce the first multi-cultural gesture dataset containing 200 individuals of 10 different cultures. In contrast to prior work, we explicitly control the emotions conveyed by the generated gestures solely through emotional speech without relying on additional conditions.

3. Method

The AMUSE pipeline consists of two separately trained networks. The audio disentanglement module, which encodes input speech into latent vectors for content, emotion, and style is described in Sec. 3.2. The main architecture is described in Sec. 3.3. It consists of a 3D human motion prior coupled with a latent diffusion model. It takes random noise (or partially denoised latent vectors) on the input and outputs a human motion sequence. We introduce broader applications in gesture editing in Sec. 3.4.

3.1. Preliminary: Expressive 3D Body Model

SMPL-X [77] is a 3D model of the body surface. SMPL-X is defined as function $M(\beta, \theta, \psi)$ that produces a 3D body mesh. It is parameterized by identity shape $\beta \in \mathbb{R}^{300}$, pose $\theta \in \mathbb{R}^{J \times 3}$ including finger articulation for rotations around J joints, and facial expression $\psi \in \mathbb{R}^{100}$. We adopt the continuous 6D rotation representation for training following Zhou et al. [114], making $\theta \in \mathbb{R}^{J \times 6}$. Given pose parameters and any shape parameter, we can obtain body mesh vertices V using the differentiable SMPL-X layer [77]. As the focus of our paper is on synthesizing body gestures and not locomotion, we disregard 8 joints that correspond those of the lower body joint poses, leaving $J = 47$. Further, we omit the facial expression parameters, i.e., set $\psi = \mathbf{0}$.

3.2. Speech Disentanglement Model

Architecture. The goal of this model is to factor an input speech into three disentangled latent representations, one for content (i.e., the words spoken), one for emotion, and one for personal style. To do so, we devise a specialized encoder-decoder architecture with three separate encoders, one for each latent space. We denote the encoders as: $E_c(a) = c$, $E_e(a) = e$, $E_s(a) = s$, where a is the input filterbank, c , e and s denote the latent vectors for content, emotion and style and E_c , E_e and E_s are their encoders. The architecture of the three encoders follows the

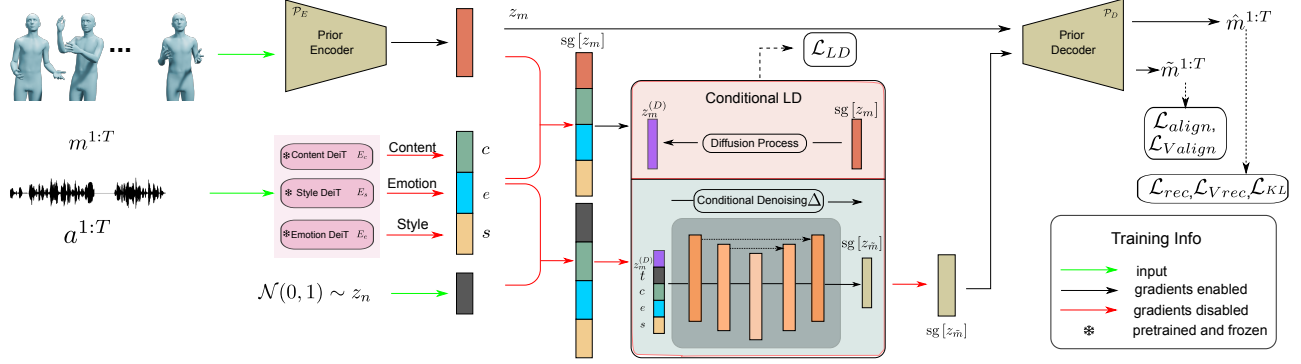


Figure 2. **Training.** We train the motion prior ($\mathcal{P}_E, \mathcal{P}_D$) and the latent denoiser Δ jointly, while keeping the audio encoding networks frozen. In the forward pass, we take an input audio $a^{1:T}$ and pose sequence $m^{1:T}$. Firstly, we do a forward pass of $m^{1:T}$ through \mathcal{P}_E and \mathcal{P}_D and compute \mathcal{L}_{rec} , \mathcal{L}_{Vrec} , and \mathcal{L}_{KL} . Then, we apply the diffusion process to a gradient-detached $sg[z_m]$ obtaining the noisy $z_m^{(D)}$, which is then denoised with Δ and \mathcal{L}_{LD} is computed. Finally, we use Δ to fully denoise z_n into gradient-detached $sg[z_{\tilde{m}}]$, further decode $\hat{m}^{1:T}$ using \mathcal{P}_D , and compute \mathcal{L}_{align} and \mathcal{L}_{Valign} .

design by Gong et al. [25, 27] (i.e., leveraging the DeiT visual transformer [98] adapted for processing filterbank images extracted from the input audio). The decoder takes the three latent vectors and produces a reconstructed filterbank. Formally $D(c, e, s) = \hat{a}$, where \hat{a} denotes the reconstructed filterbank. The decoder architecture consists of a fusion module and transformer-encoder layers.

Training. The audio module is trained with a multiple loss terms that ensure that the three latent spaces are properly disentangled. In addition to the standard autoencoder reconstruction loss, we also employ three cross-reconstruction losses, in which we enforce the correct reconstruction of the audio signal where we modify one of the content, style or emotion latents. Additionally, we employ three loss terms on the latent vector predictions – namely emotion and style classification losses over e and s , and a content similarity loss between pairs of two content latent vectors extracted from audios that have the same spoken content. For a detailed description of the encoder–decoder architecture, a formal definition of the loss functions and a detailed description of the training process please refer to the Appendix

3.3. Gesture Generation Model

Motion prior. Similar to [15, 80], our motion prior network is a VAE transformer architecture with encoder \mathcal{P}_E and decoder \mathcal{P}_D . Specifically, both \mathcal{P}_E and \mathcal{P}_D follow a U-Net-like [89] structure with skip connections between transformer blocks (see Appendix for details). The positional embeddings are learnable and injected into each multi-head attention layer, following the design of Carion et al. [13]. Formally, the encoder takes a sequence of T frames of the SMPL-X pose vectors $m^{1:T} \in \mathbb{R}^{6J \times T}$ and the first two tokens of its output, $\mu \in \mathbb{R}^{d_m}$ and $\Sigma \in \mathbb{R}^{d_m \times d_m}$ are used to extract the motion latent $z_m \in \mathbb{R}^{d_m}$ via the reparametrization trick. The decoder takes zero positional encodings as

query input and the motion latent is fed as memory to every cross-attention transformer layer, producing the reconstructed motion $\hat{m}^{1:T}$.

Diffusion process. The forward diffusion process is similar to [39, 72]. We employ fixed variance and linearly scaled noise scheduler. We add noise to the motion latent z_m for D diffusion timesteps to obtain $z_m^{(D)}$ following:

$$q(z_m^{(t_d)} | z_m^{(0)}) = \mathcal{N}(z_m^{(t_d)}; \sqrt{\bar{\alpha}_{t_d}} z_m^{(0)}, (1 - \bar{\alpha}_{t_d}) \mathbf{I}),$$

with $\alpha_{t_d} = 1 - \beta_{t_d}$, $\bar{\alpha}_{t_d} = \prod_{s=1}^{t_d} \alpha_s$, and β_{t_d} denotes diffusion process variance.

Conditional denoising process. The denoising process consists of iteratively denoising a conditioned noisy motion latent vector to obtain the denoised motion latent $z_{\tilde{m}}^{1:T}$. Our denoiser Δ is a latent variable model [88] and its architecture is similar to the U-Net-like structure of the motion prior encoder \mathcal{P}_E . The input of the model is a concatenation of: $z_m^{(t_d)}$, $SE(t_d)$, $c, e, s \in \mathbb{R}^{256}$, where $SE(t_d)$ is a sinusoidal positional encoding of diffusion timestep t_d as defined in [39]. Δ iteratively denoises through each reversed diffusion step:

$$z_m^{(t_d-1)} = \Delta([z_m^{(t_d)}, SE(t_d), c, e, s]).$$

Training. We optimize the motion prior and the latent denoiser jointly to ensure audio–motion latent code alignment during conditional fusion in the denoising process using a 3-step forward pass through the gesture generation model. First, following standard VAE practice, we reconstruct $\hat{m}^{1:T}$ by the motion prior forward pass. As shown in Fig. 2, we then disable gradient calculation in \mathcal{P}_E to infer the intermediate motion latent $sg[z_m]$, which serves as input to the denoiser. At this stage, we obtain the denoiser noise prediction, δ and use to compute the diffusion model gradients. Finally, in the third step we com-

pute $\tilde{m}^{1:T} = \mathcal{P}_D(\text{sg}[z_{\tilde{m}}])$, where $z_{\tilde{m}}$ is obtained by iteratively using the Δ to obtain a fully denoised latent from $z_n^{(t_D)} \sim \mathcal{N}(\mathbf{0}, \mathbf{I})$. We indicate computations done without gradients with a stop-gradient operation $\text{sg}[\cdot]$.

Losses. To train the motion prior, we include the standard VAE losses, namely the reconstruction loss on pose parameters \mathcal{L}_{rec} and on vertex coordinates \mathcal{L}_{Vrec} using the smooth L1 metric introduced in [24], which we denote as L_1^s :

$$\mathcal{L}_{rec} = L_1^s(m^{1:T}, \hat{m}^{1:T}), \quad \mathcal{L}_{Vrec} = L_1^s(V^{1:T}, \hat{V}^{1:T}),$$

where the root-centered vertices V are obtained by feeding in pose parameters m to a differentiable SMPL-X layer (without learnable parameters) and a mean shape $\beta = \bar{0}$. The KL divergence loss of the motion prior is:

$$\mathcal{L}_{KL} = \frac{1}{2} \left[\sum_{i=1}^z (\mu_i^2 + \sigma_i^2) - \sum_{i=1}^z (\log(\sigma_i^2) + 1) \right].$$

To ensure the alignment of the diffusion-generated motions and the input audio, we apply the alignment reconstruction loss on the inferred motion pose parameters and the vertex coordinates:

$$\mathcal{L}_{align} = L_1^s(m^{1:T}, \tilde{m}^{1:T}), \quad \mathcal{L}_{Valign} = L_1^s(V^{1:T}, \tilde{V}^{1:T}).$$

Finally, we utilize the objective similar to [15, 39, 88] to supervise the denoiser:

$$\mathcal{L}_{LD} = \left\| \delta^{(t_d)} - \Delta(z_m^{(t_d)}, \text{SE}(t_d), c, e, s) \right\|_2^2,$$

where $\delta^{(t_d)}$ is the noise vector sampled from $\mathcal{N}(\mathbf{0}, \mathbf{I})$ in the corresponding diffusion step t_d . The combined gesture model loss is:

$$\mathcal{L}_{ges} = \mathcal{L}_{rec} + \mathcal{L}_{Vrec} + \mathcal{L}_{KL} + \mathcal{L}_{align} + \mathcal{L}_{Valign} + \mathcal{L}_{LD}$$

Inference. We employ DDIM [94] to infer high quality conditional motion samples with a small number of denoising timesteps. During inference we draw a sample vector from $\mathcal{N}(\mathbf{0}, \mathbf{I})$ to iteratively denoise in reversed timesteps. The denoised sample is then passed through the decoder $\mathcal{P}_D(z_{\tilde{m}^{1:T}})$ to obtain motion $\tilde{m}^{1:T}$.

3.4. Gesture Editing

Due to the disentangling of the inputs, AMUSE achieves semantic gesticulation control using two driving input audios. Specifically, given two input audio signals a_1 and a_2 , we extract their latent representations of content c_1, c_2 , emotion e_1, e_2 , and style s_1, s_2 . Then, we simply initialize the denoising procedure of Δ with the triplet (c_1, e_2, s_1) , generating the gesture with the content and style of a_1 but the emotion of input audio a_2 . Similarly, instead of emotion we can also change the gesticulation style to that of the speaker of a_2 by initializing with (c_1, e_1, s_2) .

4. Implementation Details

MoCap data preparation. The BEAT [58] mocap sequences, captured in a Vicon system at 120 Hz, are down-sampled to 30 Hz and processed using MoSh++ [61, 65] to obtain SMPL-X parameters. Given a sequence of 3D mocap marker positions, we jointly optimize SMPL-X shape and pose parameters, 3D body translation, and embedding of the mocap markers in the SMPL-X surface. Once processed, the sequences are then divided according to the emotion annotations in the BEAT dataset. We use sequences of English speaking subjects in monologue speaking style for training and evaluating AMUSE. For each sequence we draw $m^{1:L}$ at 30 FPS and concatenate with audio content c , emotion e , and style s latent vectors. Then, we segment it to 10-sec windows T , beginning from the timestamp 0 and discarding additional unaligned information at the end. This pre-processing choice allows us to train transformer networks without masking. We provide additional data processing information in the Appendix

Audio preprocessing. We use audio sequences belonging to eight categorical emotion labels (neutral, happy, angry, sad, contempt, surprise, fear, and disgust). Each audio chunk of 10s is converted into a filter bank with 128 mel-frequency bins with a 25ms Hamming frame window and 10ms frame shift. We mask each sample with a maximum length of 24 in the frequency domain and a maximum length of 96 in the time domain, employing Park et al. [76]. Following [25, 27], we standardize the filter bank and augment it via noise injection and circular shifting. Before feeding in our speech disentanglement model, each filter bank is split into a sequence of fixed 1209 patches of 16 x 16 each having 6 units overlap in frequency and time domain.

Motion prior. The motion prior is a VAE encoder–decoder with 9 layers and 4 heads, following Chen et al. [15]. The encoder–decoder is a U-Net-like transformer with residual connections. Learnable positional embeddings are injected in each multi-head attention layer. We have a linear projection at the start and the end of our motion prior network. The KL divergence term is weighted with a factor of $1e-4$.

Denoiser. The denoiser follows the same network architecture as our prior encoder. The hidden dimension of all transformer layers is 1024. We use 1000 diffusion steps D during training and 50 during inference. Noise betas are in range [0.00085, 0.012]. We jointly optimize the prior and denoiser networks for 5000 epochs with batch size of 64, learning rate 0.0001, and the AdamW optimizer [62].

5. Experiments

Speech disentanglement model. We evaluate the performance of the speech disentanglement model quantitatively using classification accuracy and F1 scores on emotion and style. The accuracy is computed as average scores for

all 8 emotion as well style categories that are part of the test dataset. The emotion and style accuracy is 91.53% and 96.06%, respectively. The emotion F1 score and style F1 scores are 0.914 and 0.960, respectively. See the Appendix for ablations and a detailed metric analysis.

Gesture generation model. We evaluate the performance of our gesture generation model quantitatively, qualitatively, and perceptually against following methods: TalkSHOW [107] and the re-implementation of Habibie et al. [34] provided by the TalkSHOW authors in the official TalkSHOW release [106], DiffuseStyleGesture (DSG) [103], MoGlow [37], and CaMN [58]. Additionally, we adapt TalkSHOW to include categorical emotion labels as input along with the existing architecture that only allows one-hot encodings of personal style. We then retrain it on our training data. We refer to it as TalkSHOW-BEAT. There are some concurrent works [5, 7, 59], which introduce methods for gesture generation from speech, however, direct comparison is hindered by the unavailability of released code our task. Refer to the Appendix for the ablation experiments, the emotion and style editing experiments, and their quantitative evaluation.

5.1. Quantitative Evaluation

To quantitatively evaluate our method’s gesture generations and edited gesture generations, we train a transformer-based encoder architecture (denoted as M) similar to Petrovich et al. [80] in an autoencoder setting, where we append a CLS token at the beginning of the motion sequence. M is trained with a cross-entropy emotion classification objective applied to the output CLS token. We train M on the BEAT training dataset and use its features to compute the following metrics: (1) Fréchet gesture distance (FGD): We

follow [93, 109, 110] to compute the feature distance between generated and ground truth motion features. (2) Gesture diversity (Div): Similarly to Chen et al. [15], we compute variance across generated features. (3) Gesture emotion accuracy (GA): We report top-1 emotion classification accuracy predicted by a classifier trained on the motion M -predicted latents. (4) Beat align (BA): We follow [54, 58], to evaluate the motion-speech correlation in terms of the similarity between the kinematic motion beats and speech audio beats. The kinematic motion beats are directly computed from the generated motion sequences. (5) Semantic-Relevant Gesture Recall (SRGR): We follow Liu et al. [58], to evaluate the semantic relevancy of gestures with GT motion. We use the ground truth semantic scores to compute this metric. The scores are obtained from the BEAT authors, representing a continuous score on a scale 0-1 per gesture style for 4 gesture semantic categories: beat, deictic, iconic, and metaphoric. While comparing with methods that output coarse skeletal data (DSG [103], MoGlow [37], and CaMN [58]), we convert the skeleton motion data into the SMPL-X axis angle representation. For details on the architectures and training of M , and the losses, please refer to the Appendix

We prepare the evaluation data by randomly selecting 72 unique motion sequences each of length 10s and comprising 8 emotions across test subjects and compute the aforementioned metrics. We use 9 sequences for each emotion per subject. The results are reported in Tab. 1. All best scores are highlighted in green and second best in blue. AMUSE outperforms the baseline methods in all given metrics. To validate the performance of gesture emotion editing, we also report the same metrics for the emotion editing task (Ours-EmoEdit). During inference, the input style and content latents are extracted from neutral-emotion audio, while the emotion latent comes from a different audio of different emotion. These emotional edits offer numerous possibilities, allowing for transitions from any to any emotion. Tab. 1 shows the average for editing from neutral to other emotions. Since we require the GT gesture semantics score to compute SRGR metric, it is not possible to compute the SRGR for the synthetic edited-emotion gestures as they are not part of the original BEAT dataset. Ours-EmoEdit outperforms the baseline methods in BA, Div, and GA metrics. This demonstrates the capability of our model to maintain highly discriminative cues when switching between different emotions. TalkSHOW-BEAT has the second best score for SRGR whereas TalkSHOW demonstrates second best FGD score. Although, our model and ours-EmoEdit show improvements over the baseline methods, GT motions have higher diversity, Beat alignment score, and are easier to classify than generations of AMUSE, highlighting the challenging nature of the problem.

Method	SRGR \uparrow	BA \uparrow	FGD \downarrow	Div \rightarrow	GA \uparrow^a
GT	—	0.83	—	27.83	64.04
Ours	0.36	0.81	388.63	25.06	46.76
Ours-EmoEdit ^b	—	0.79	792.58	24.68	34.18
TalkSHOW-BEAT	0.31	0.64	808.99	24.16	22.71
TalkSHOW [107]	0.30	0.60	762.15	23.19	29.41
DSG [103]	0.23	0.40	763.10	19.77	22.70
Habibie et al. [34]	0.23	0.39	809.17	21.34	16.67
MoGlow [37]	0.21	0.35	1097.03	19.50	16.62
CaMN [58]	0.21	0.39	1063.87	18.90	14.17

^a GA is average of all 8 emotions.

^b GA for these are average accuracy for all generations with 7 edited audio sequences.

Table 1. **Gesture quantitative results.** We compare our methods against several SOTA methods using metrics explained in Sec. 5.1. We observe that AMUSE outperforms in all scores compared to baseline methods. Additionally, AMUSE-EmoEdit outperforms in Beat Align, Diversity, and Gesture Emotion Accuracy scores compared to the baseline methods.

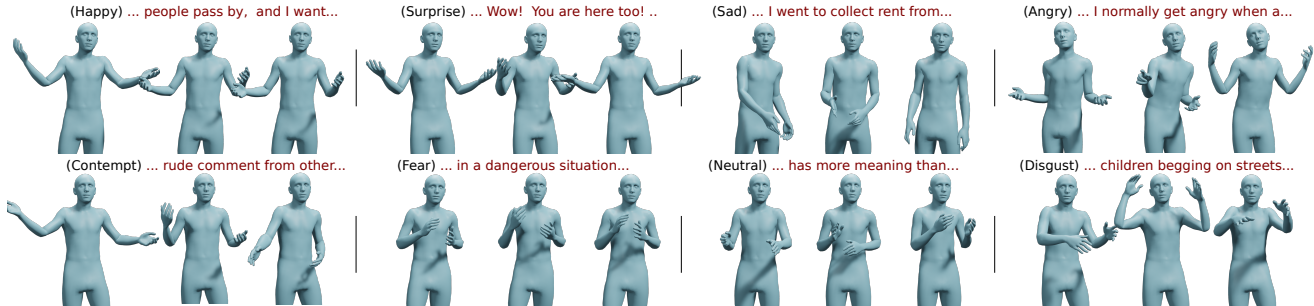


Figure 3. **Qualitative comparison across all emotions.** We evaluate generation on different test audios. AMUSE exhibits well-synchronized beat gestures and consistently produces gestures that accurately convey the emotional content expressed in the input speech.

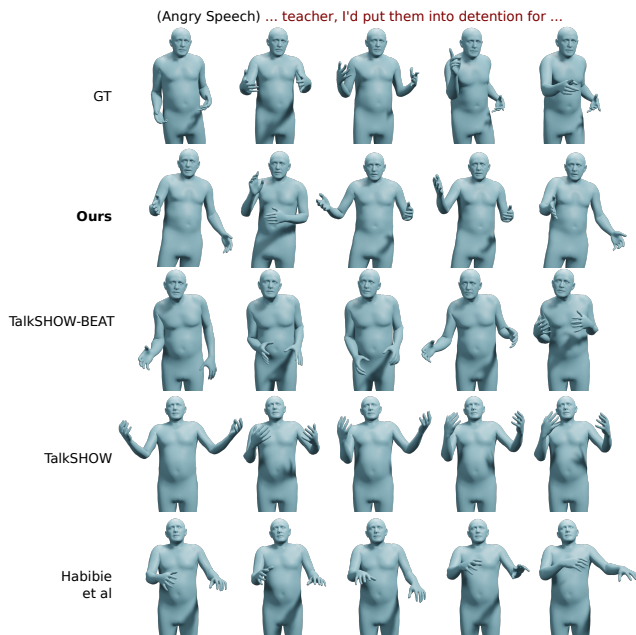


Figure 4. **Qualitative comparison with baseline methods.** The speech segment describes intense angry speech.

5.2. Qualitative Evaluation

Comparison with baseline methods. In Fig. 4, we demonstrate comparison with baseline methods that output a 3D body mesh: Habibie et al. [34], TalkSHOW [107], TalkSHOW-BEAT, and the BEAT ground truth (GT) [58]. We observe that AMUSE generates gestures that are semantically closer to the speech content and produces expressive emotional gestures closer to the perceived emotion. For example, the GT motion exhibits anger when saying “*put them into detention*”. AMUSE demonstrates tense posture and aggressive movements comparable with the ground truth data and accurate synchronization with the spoken words. TalkSHOW [107] and Habibie et al. [34] exhibit limited movement and display inferior and static gestures on test audios as seen in the last two rows



Figure 5. **Qualitative evaluation of diverse generations.** Multiple generations overlaid.

of Fig. 4. TalkSHOW-BEAT slightly outperforms other baseline methods by demonstrating enhanced synchronized gestures, but it still does not perform as well as AMUSE.

Diverse emotional gestures. In Fig. 5, our probabilistic model can generate diverse gestures for same input audio.

Emotional gesture generation. In Fig. 3 AMUSE demonstrates strong correlation with the spoken utterances as well as different emotions. We observe that our model is able to correlate semantic words to associated gestures. For example, gestures demonstrate forceful actions and tense stance with angry audio “*normally get angry*” whereas it generates lowered and calm hand positions for sad audio “*I went to collect*”. Similarly, our generations show hands that are closer to body for fearful audio “*in a dangerous situation*” while widely open expressing astonishment for happy and surprised audio “*people pass by*” and “*Wow! You are here*”.

Emotion editing. We use two audio streams of a female subject for neutral and sad emotion. This experiment edits the subject’s gesture style from moderately controlled hand movements to a sad style with lethargic posture conveying a sense of heaviness, as seen in Fig. 7 (top).

Gesture style editing. We use audio streams of two male subjects for the happy (ID - 13) and angry (ID - 2) emotion. With the emotion, style and content latent fusion mechanism from two driving audio streams, AMUSE is able to adapt the male (ID - 13) subject’s body gestures from being close to their body to more open with squared tightened shoulders, expressing a shift from happy to angry emotions of a different subject (ID - 2), as shown in Fig. 7 (bottom). Please refer to the supplemental video for qualitative results and comparisons to additional gesture genera-

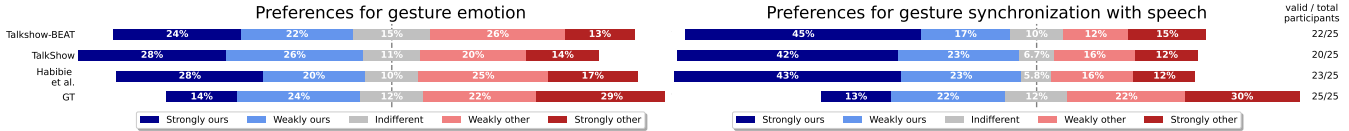


Figure 6. The perceptual study results for gesture emotion preference (left) and synchronization with speech (right). The number of attentive participants that passed the catch trials is indicated on the right and the reported results only consider these participants.

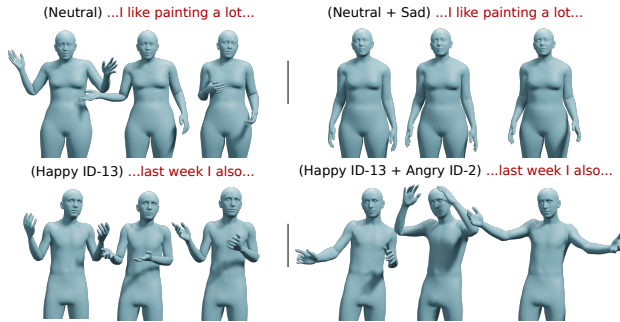


Figure 7. **Gesture editing.** Top: We modify style from being neutral (left) to being sad (right) by combining the emotion latent from sad audio with the content latent from neutral audio. Bottom: We transform the style from Subject 13 being happy (left) to being angry (right) by merging the content latent from happy audio with the style and emotion latents from an angry audio of Subject 2.

tion methods [4, 58, 116] trained on coarse skeletal data.

5.3. Perceptual Study

Design. Our perceptual study is designed as a side-by-side comparison of two gesture videos generated with the same audio as input but by two different methods (AMUSE and another model or GT). The participants are asked to rate their preference of the methods on a five-point Likert scale for “synchronization with speech” and “gesture emotion appropriateness” given the GT emotion label of the input audio. We recruit 25 participants per method-to-method comparison on Amazon Mechanical Turk. Each participant is shown 24 pairs of randomly selected test set animations, 3 per emotion (neutral, happy, angry, sad, disgust, fear, surprise, and contempt). To allow the participant to get used to the task, we discard the answers of the first three comparisons and repeat these at the end. We incorporate three catch trials and responses from participants that fail on more than one are filtered out, as shown in Fig. 6 (right).

Results. The results of the study are shown in Fig. 6. AMUSE outperforms all competing methods by a considerable margin on both tasks, suggesting that AMUSE’s generations are more appropriate for both the content of the input speech and its emotion compared to the baselines. However, it must be noted that there is still a significant gap between AMUSE and the GT. Please refer to the Appendix for details about the perceptual study.

5.4. Discussion and Future Work

Upper-body motion. We focus on the smooth coordination between the pelvis and upper body animation for side-by-side comparisons with other methods, as all other methods primarily focus on upper body movements. Future work should include lower-body motion and locomotion as these impact the perceived emotional state of a sequence.

Semantics. While the generated gestures, synchronized with the driving speech sequence, do not account for semantics such as deictic and metaphoric gestures, incorporating the text/language modality could help further improve in this direction.

Facial expressions. While emotional speech-driven face animation methods [18, 78] can be combined with bodies generated from AMUSE, jointly learning to generate emotional 3D bodies from speech is a topic that needs attention.

End-to-end training. Joint audio-gesture training may enhance results but requires careful loss term balancing and increased GPU memory. Therefore, we opted for separate training.

6. Conclusion

We present AMUSE, a framework to generate emotional body gestures from speech. The emotions and personal styles of the synthesized gestures can be controlled, thanks to the disentanglement of content, emotion, and style directly from the speech. The latent diffusion-based framework can further generate variations of the same gesture with the same emotion. Our quantitative evaluations show that AMUSE achieves state of the art performance on a variety of metrics: diversity, gesture emotion classification accuracy, Fréchet gesture distance, beat alignment score, and semantic relevant gesture recall. Finally, our perceptual study demonstrates that AMUSE generates motions that are better synchronized and better match the emotion expressed of the input speech than previous state of the art.

Acknowledgments. We thank A Cseke, T McConnell and T Alexiadis for help with the perceptual study, B Pellkofer, J Piles-Contreras, and E Fritzler for IT support, and P Kulits, M Petrovich, S Kokane, and S Zojaji for proofreading and insightful discussions. This project has received funding from the European Union’s Horizon 2020 research and innovation programme under the Marie Skłodowska-Curie grant agreement No. 860768.

Disclosure. <https://download.is.tue.mpg.de/amuse/Disclosure.txt>

References

- [1] Kfir Aberman, Yijia Weng, Dani Lischinski, Daniel Cohen-Or, and Baoquan Chen. Unpaired motion style transfer from video to animation. *Transactions on Graphics (TOG)*, 2020. [3](#)
- [2] Chaitanya Ahuja and Louis-Philippe Morency. Language2Pose: Natural language grounded pose forecasting. *International Conference on 3D Vision (3DV)*, 2019. [2](#)
- [3] Chaitanya Ahuja, Dong Won Lee, and Louis-Philippe Morency. Low-resource adaptation for personalized co-speech gesture generation. In *Computer Vision and Pattern Recognition (CVPR)*, pages 20566–20576, 2022. [2](#)
- [4] Simon Alexanderson, Gustav Eje Henter, Taras Kucherenko, and Jonas Beskow. Style-controllable speech-driven gesture synthesis using normalising flows. *Computer Graphics Forum (CGF)*, 39(2):487–496, 2020. [3](#), [8](#), [16](#), [17](#)
- [5] Simon Alexanderson, Rajmund Nagy, Jonas Beskow, and Gustav Eje Henter. Listen, Denoise, Action! Audio-driven motion synthesis with diffusion models. *Transactions on Graphics (TOG)*, 42(4):1–20, 2023. [1](#), [3](#), [6](#), [20](#)
- [6] Tenglong Ao, Qingzhe Gao, Yuke Lou, Baoquan Chen, and Libin Liu. Rhythmic gesticulator. *Transactions on Graphics (TOG)*, 41(6):1–19, 2022. [3](#)
- [7] Tenglong Ao, Zeyi Zhang, and Libin Liu. GestureDiffu-CLIP: Gesture diffusion model with CLIP latents. *Transactions on Graphics (TOG)*, 2023. [1](#), [3](#), [6](#), [20](#)
- [8] Nikos Athanasiou, Mathis Petrovich, Michael J. Black, and Gül Varol. TEACH: Temporal Action Compositions for 3D Humans. In *International Conference on 3D Vision (3DV)*, 2022. [2](#)
- [9] Nikos Athanasiou, Mathis Petrovich, Michael J. Black, and Gül Varol. SINC: Spatial composition of 3D human motions for simultaneous action generation. *International Conference on Computer Vision (ICCV)*, 2023. [2](#)
- [10] Emad Barsoum, John Kender, and Zicheng Liu. HP-GAN: probabilistic 3d human motion prediction via GAN. In *Computer Vision and Pattern Recognition Workshops (CVPRW)*, 2017. [2](#)
- [11] Uttaran Bhattacharya, Elizabeth Childs, Nicholas Rewkowski, and Dinesh Manocha. Speech2affectivegestures: Synthesizing co-speech gestures with generative adversarial affective expression learning. In *ACM International Conference on Multimedia (MM)*, 2021. [3](#)
- [12] Uttaran Bhattacharya, Nicholas Rewkowski, Abhishek Banerjee, Pooja Guhan, Aniket Bera, and Dinesh Manocha. Text2gestures: A transformer-based network for generating emotive body gestures for virtual agents. In *IEEE Virtual Reality and 3D User Interfaces, VR*, 2021. [3](#)
- [13] Nicolas Carion, Francisco Massa, Gabriel Synnaeve, Nicolas Usunier, Alexander Kirillov, and Sergey Zagoruyko. End-to-end object detection with transformers. In *European Conference on Computer Vision (ECCV)*, pages 213–229. Springer, 2020. [4](#)
- [14] Justine Cassell, Hannes Högni Vilhjálmsson, and Timothy Bickmore. *BEAT: The Behavior Expression Animation Toolkit*, pages 163–185. Springer, 2004. [2](#)
- [15] Xin Chen, Biao Jiang, Wen Liu, Zilong Huang, Bin Fu, Tao Chen, and Gang Yu. Executing your commands via motion diffusion in latent space. In *Computer Vision and Pattern Recognition (CVPR)*, pages 18000–18010, 2023. [4](#), [5](#), [6](#), [17](#)
- [16] Enric Corona, Albert Pumarola, G. Alenyà, and F. Moreno-Noguer. Context-aware human motion prediction. In *Computer Vision and Pattern Recognition (CVPR)*, pages 6990–6999, 2020. [2](#)
- [17] Rishabh Dabral, Muhammad Hamza Mughal, Vladislav Golyanik, and Christian Theobalt. Mofusion: A framework for denoising-diffusion-based motion synthesis. In *Computer Vision and Pattern Recognition (CVPR)*, 2023. [2](#)
- [18] Radek Daněček, Kiran Chhatre, Shashank Tripathi, Yandong Wen, Michael Black, and Timo Bolkart. Emotional speech-driven animation with content-emotion disentanglement. In *International Conference on Computer Graphics and Interactive Techniques in Asia (SIGGRAPH ASIA)*, 2023. [2](#), [3](#), [8](#)
- [19] Paul Ekman. Facial expression and emotion. *American Psychologist*, 48(4):384–392, 1993. [1](#)
- [20] Esam Ghaleb, Ilya Burenko, Marlou Rasenberg, Wim Pouw, Peter Uhrig, Judith Holler, Ivan Toni, Aslı Özyürek, and Raquel Fernández. Co-speech gesture detection through multi-phase sequence labeling. In *Winter Conference on Applications of Computer Vision (WACV)*, 2024. [3](#)
- [21] Saeed Ghorbani, Ylva Ferstl, Daniel Holden, Nikolaus F. Troje, and Marc-André Carboneau. Zeroeggs: Zero-shot example-based gesture generation from speech. *Computer Graphics Forum (CGF)*, 42(1):206–216, 2023. [3](#), [19](#)
- [22] Anindita Ghosh, Noshaba Cheema, Cennet Oguz, Christian Theobalt, and Philipp Slusallek. Synthesis of compositional animations from textual descriptions. In *International Conference on Computer Vision (ICCV)*, 2021. [2](#)
- [23] Shiry Ginosar, Amir Bar, Gefen Kohavi, Caroline Chan, Andrew Owens, and Jitendra Malik. Learning individual styles of conversational gesture. In *Computer Vision and Pattern Recognition (CVPR)*, pages 3497–3506, 2019. [2](#)
- [24] Ross B. Girshick. Fast R-CNN. In *International Conference on Computer Vision (ICCV)*, pages 1440–1448, 2015. [5](#)
- [25] Yuan Gong, Yu-An Chung, and James R. Glass. AST: audio spectrogram transformer. In *Interspeech 2021*, pages 571–575, 2021. [4](#), [5](#), [13](#), [14](#)
- [26] Yuan Gong, Yu-An Chung, and James Glass. PSLA: Improving audio tagging with pretraining, sampling, labeling, and aggregation. *IEEE/ACM Transactions on Audio, Speech, and Language Processing*, 29:3292–3306, 2021.
- [27] Yuan Gong, Cheng-I Lai, Yu-An Chung, and James R. Glass. SSAST: self-supervised audio spectrogram transformer. In *AAAI Conference on Artificial Intelligence*, pages 10699–10709, 2022. [4](#), [5](#), [14](#)
- [28] Daniel Grzywczak and Grzegorz Gwardys. Deep image features in music information retrieval. *International Journal of Electronics and Telecommunications*, 60:187–199, 2014. [13](#)

- [29] Chuan Guo, Xinxin Zuo, Sen Wang, Shihao Zou, Qingyao Sun, Annan Deng, Minglun Gong, and Li Cheng. Action2Motion: Conditioned generation of 3d human motions. In *ACM International Conference on Multimedia (MM)*, 2020. 2
- [30] Chuan Guo, Shihao Zou, Xinxin Zuo, Sen Wang, Wei Ji, Xingyu Li, and Li Cheng. Generating diverse and natural 3D human motions from text. In *Computer Vision and Pattern Recognition (CVPR)*, 2022. 2
- [31] Andrey Guzhov, Federico Raue, Jörn Hees, and Andreas Dengel. Esresnet: Environmental sound classification based on visual domain models. In *International Conference on Pattern Recognition (ICPR)*, pages 4933–4940. IEEE, 2020. 13
- [32] Nejla Gürefe. The role of gestures in mathematical discourse of hard-hearing students: Prism example. *Acta Didactica Napocensia*, 11:125–140, 2018. 1
- [33] I. Habibie, Daniel Holden, Jonathan Schwarz, J. Yearsley, and T. Komura. A recurrent variational autoencoder for human motion synthesis. In *British Machine Vision Conference (BMVC)*, 2017. 2
- [34] Ikhsanul Habibie, Weipeng Xu, Dushyant Mehta, Lingjie Liu, Hans-Peter Seidel, Gerard Pons-Moll, Mohamed Elgharib, and Christian Theobalt. Learning speech-driven 3d conversational gestures from video. In *ACM International Conference on Intelligent Virtual Agents (IVA)*, 2021. 1, 6, 7
- [35] Ikhsanul Habibie, Mohamed A. Elgharib, Kripasindhu Sarkar, Ahsan Abdullah, Simbarashe Linval Nyatsanga, Michael Neff, and Christian Theobalt. A motion matching-based framework for controllable gesture synthesis from speech. *International Conference on Computer Graphics and Interactive Techniques (SIGGRAPH)*, 2022. 2
- [36] Félix G. Harvey, Mike Yurick, Derek Nowrouzezahrai, and Christopher Joseph Pal. Robust motion in-betweening. *Transactions on Graphics (TOG)*, 2020. 2
- [37] Gustav Eje Henter, Simon Alexanderson, and Jonas Beskow. MoGlow: Probabilistic and controllable motion synthesis using normalising flows. *Transactions on Graphics (TOG)*, 39(4):236:1–236:14, 2020. 3, 6, 20
- [38] Sandra Herbert. Gesture types for functions. *Mathematics Education Research Group of Australasia*, pages 322–329, 2012. 1
- [39] Jonathan Ho, Ajay Jain, and Pieter Abbeel. Denoising diffusion probabilistic models. In *Conference on Neural Information Processing Systems (NeurIPS)*, 2020. 4, 5
- [40] Xun Huang and Serge J. Belongie. Arbitrary style transfer in real-time with adaptive instance normalization. In *International Conference on Computer Vision (ICCV)*, pages 1510–1519, 2017. 3
- [41] Tero Karras, Timo Aila, Samuli Laine, Antti Herva, and Jaakko Lehtinen. Audio-driven facial animation by joint end-to-end learning of pose and emotion. *Transactions on Graphics (TOG)*, 2017. 3
- [42] Adam Kendon. *Gesture: Visible action as utterance*. Cambridge University Press, 2004. 1
- [43] Gwantae Kim, Seonghyeok Noh, Insung Ham, and Hanseok Ko. MPE4G : Multimodal pretrained encoder for co-speech gesture generation. In *International Conference on Acoustics, Speech and Signal Processing (ICASSP)*, pages 1–5, 2023. 2
- [44] Jihoon Kim, Taehyun Byun, Seungyoung Shin, Jungdam Won, and Sungjoon Choi. Conditional motion in-betweening. *Pattern Recognition*, 2022. 2
- [45] Chris L Kleinke. Gaze and eye contact: A research review. *Psychological Bulletin*, 100(1):78–100, 1986. 1
- [46] Zhifeng Kong, Wei Ping, Jiaji Huang, Kexin Zhao, and Bryan Catanzaro. DiffWave: A versatile diffusion model for audio synthesis. In *International Conference on Learning Representations (ICLR)*, 2021. 3
- [47] Stefan Kopp, Brigitte Krenn, Stacy Marsella, Andrew N. Marshall, Catherine Pelachaud, Hannes Pirker, Kristinn R. Thórisson, and Hannes Vilhjálmsón. Towards a common framework for multimodal generation: The behavior markup language. In *Intelligent Virtual Agents (IVA)*, pages 205–217. Springer, 2006. 2
- [48] Quoc Anh Le, Souheil Hanoune, and Catherine Pelachaud. Design and implementation of an expressive gesture model for a humanoid robot. In *IEEE-RAS International Conference on Humanoid Robots*, pages 134–140, 2011. 2
- [49] Gilwoo Lee, Zhiwei Deng, Shugao Ma, Takaaki Shiratori, Siddhartha S. Srinivasa, and Yaser Sheikh. Talking With Hands 16.2M: A large-scale dataset of synchronized body-finger motion and audio for conversational motion analysis and synthesis. In *International Conference on Computer Vision (ICCV)*, pages 763–772, 2019. 2
- [50] Robert W Levenson. Blood, sweat, and fears: The autonomic architecture of emotion. *Annals of the New York Academy of Sciences*, 1000:348–366, 2003. 1
- [51] Jing Li, Di Kang, Wenjie Pei, Xuefei Zhe, Ying Zhang, Zhenyu He, and Linchao Bao. Audio2gestures: Generating diverse gestures from speech audio with conditional variational autoencoders. In *Computer Vision and Pattern Recognition (CVPR)*, pages 11293–11302, 2021. 2
- [52] Peizhuo Li, Kfir Aberman, Zihan Zhang, Rana Hanocka, and Olga Sorkine-Hornung. GANimator: Neural motion synthesis from a single sequence. *Transactions on Graphics (TOG)*, 2022. 2
- [53] Ruilong Li, Shan Yang, D. A. Ross, and Angjoo Kanazawa. AI choreographer: Music conditioned 3D dance generation with AIST++. In *International Conference on Computer Vision (ICCV)*, 2021. 2, 18
- [54] Ruilong Li, Shan Yang, David A. Ross, and Angjoo Kanazawa. AI choreographer: Music conditioned 3d dance generation with AIST++. In *International Conference on Computer Vision (ICCV)*, pages 13381–13392, 2021. 6
- [55] William Li and Philippe Pasquier. Automatic affect classification of human motion capture sequences in the valence-arousal model. In *International Symposium on Movement and Computing*, 2016. 3
- [56] Yuanzhi Liang, Qianyu Feng, Linchao Zhu, Li Hu, Pan Pan, and Yi Yang. Seeg: Semantic energized co-speech gesture generation. In *Computer Vision and Pattern Recognition (CVPR)*, 2022. 2

- [57] Haiyang Liu, Naoya Iwamoto, Zihao Zhu, Zhengqing Li, You Zhou, Elif Bozkurt, and Bo Zheng. DisCo: Disentangled implicit content and rhythm learning for diverse co-speech gestures synthesis. In *ACM International Conference on Multimedia (MM)*, pages 3764–3773, 2022. [3](#)
- [58] Haiyang Liu, Zihao Zhu, Naoya Iwamoto, Yichen Peng, Zhengqing Li, You Zhou, Elif Bozkurt, and Bo Zheng. BEAT: A large-scale semantic and emotional multi-modal dataset for conversational gestures synthesis. *European Conference on Computer Vision (ECCV)*, 2022. [2](#), [3](#), [5](#), [6](#), [7](#), [8](#), [16](#), [17](#), [18](#), [19](#)
- [59] Haiyang Liu, Zihao Zhu, Giorgio Becherini, Yichen Peng, Mingyang Su, You Zhou, Xuefei Zhe, Naoya Iwamoto, Bo Zheng, and Michael J. Black. EMAGE: Towards unified holistic co-speech gesture generation via expressive masked audio gesture modeling. In *Computer Vision and Pattern Recognition (CVPR)*, 2024. [1](#), [2](#), [6](#)
- [60] Yuejiang Liu, Riccardo Cadei, Jonas Schweizer, Sherwin Bahmani, and Alexandre Alahi. Towards robust and adaptive motion forecasting: A causal representation perspective. In *Computer Vision and Pattern Recognition (CVPR)*, 2022. [2](#)
- [61] Matthew M. Loper, Naureen Mahmood, and Michael J. Black. MoSh: Motion and shape capture from sparse markers. *Transactions on Graphics (TOG)*, 33(6):220:1–220:13, 2014. [5](#), [19](#)
- [62] Ilya Loshchilov and Frank Hutter. Decoupled weight decay regularization. In *International Conference on Learning Representations (ICLR)*, 2019. [5](#)
- [63] Shuhong Lu, Youngwoo Yoon, and Andrew W. Feng. Co-speech gesture synthesis using discrete gesture token learning. *International Conference on Intelligent Robots and Systems (IROS)*, pages 9808–9815, 2023. [2](#)
- [64] Birgit Lugin, Catherine Pelachaud, and David Traum, editors. *The Handbook on Socially Interactive Agents: 20 Years of Research on Embodied Conversational Agents, Intelligent Virtual Agents, and Social Robotics Volume 1: Methods, Behavior, Cognition*. 2021. [1](#)
- [65] Naureen Mahmood, Nima Ghorbani, Nikolaus F. Troje, Gerard Pons-Moll, and Michael J. Black. Amass: Archive of motion capture as surface shapes. In *International Conference on Computer Vision (ICCV)*, 2019. [2](#), [5](#), [19](#)
- [66] Stacy Marsella, Yuyu Xu, Margaux Lhomme, Andrew Feng, Stefan Scherer, and Ari Shapiro. Virtual character performance from speech. In *SIGGRAPH/Eurographics Symposium on Computer Animation (SCA)*, page 25–35, 2013. [2](#)
- [67] Julieta Martinez, Michael J. Black, and Javier Romero. On human motion prediction using recurrent neural networks. In *Computer Vision and Pattern Recognition (CVPR)*, 2017. [2](#)
- [68] David McNeill. Hand and mind: What gestures reveal about thought. *Bibliovault OAI Repository, the University of Chicago Press*, 27, 1994. [1](#)
- [69] Albert Mehrabian. *Nonverbal communication*. Aldine-Atherton Chicago, 1972. [1](#)
- [70] Shivam Mehta, Siyang Wang, Simon Alexanderson, Jonas Beskow, Éva Székely, and Gustav Eje Henter. Diff-TTSG: Denoising probabilistic integrated speech and gesture synthesis. In *Proc. ISCA Speech Synthesis Workshop (SSW)*, pages 150–156, 2023. [2](#)
- [71] Davide Moltisanti, Jinyi Wu, Bo Dai, and Chen Change Loy. BRACE: the breakdancing competition dataset for dance motion synthesis. In *European Conference on Computer Vision (ECCV)*, pages 329–344, 2022. [2](#)
- [72] Alexander Quinn Nichol and Prafulla Dhariwal. Improved denoising diffusion probabilistic models. In *International Conference on Machine Learning (ICML)*, pages 8162–8171, 2021. [4](#)
- [73] Dirk Ormoneit, Michael J. Black, T. Hastie, and H. Kjellström. Representing cyclic human motion using functional analysis. *Image and Vision Computing (IVC)*, 2005. [2](#)
- [74] Kamalesh Palanisamy, Dipika Singhanian, and Angela Yao. Rethinking cnn models for audio classification. *arXiv:2007.11154*, 2020. [13](#)
- [75] Kunkun Pang, Dafei Qin, Yingruo Fan, Julian Habekost, Takaaki Shiratori, Junichi Yamagishi, and Taku Komura. BodyFormer: Semantics-guided 3d body gesture synthesis with transformer. *Transactions on Graphics (TOG)*, 42(4), 2023. [2](#), [19](#)
- [76] Daniel S. Park, William Chan, Yu Zhang, Chung-Cheng Chiu, Barret Zoph, Ekin D. Cubuk, and Quoc V. Le. SpecAugment: A simple data augmentation method for automatic speech recognition. In *Interspeech 2019. ISCA*, 2019. [5](#)
- [77] Georgios Pavlakos, Vasileios Choutas, Nima Ghorbani, Timo Bolkart, Ahmed A. A. Osman, Dimitrios Tzionas, and Michael J. Black. Expressive body capture: 3D hands, face, and body from a single image. In *Computer Vision and Pattern Recognition (CVPR)*, pages 10975–10985, 2019. [2](#), [3](#)
- [78] Ziqiao Peng, Haoyu Wu, Zhenbo Song, Hao Xu, Xiangyu Zhu, Jun He, Hongyan Liu, and Zhaoxin Fan. EmoTalk: Speech-driven emotional disentanglement for 3d face animation. In *International Conference on Computer Vision (ICCV)*, pages 20687–20697, 2023. [2](#), [3](#), [8](#)
- [79] Mathis Petrovich, Michael J. Black, and Gül Varol. Action-conditioned 3D human motion synthesis with transformer VAE. In *International Conference on Computer Vision (ICCV)*, 2021. [2](#)
- [80] Mathis Petrovich, Michael J. Black, and Gül Varol. Action-conditioned 3D human motion synthesis with transformer VAE. In *International Conference on Computer Vision (ICCV)*, 2021. [4](#), [6](#), [17](#)
- [81] Mathis Petrovich, Michael J. Black, and Gül Varol. TEMOS: Generating diverse human motions from textual descriptions. In *European Conference on Computer Vision (ECCV)*, 2022. [2](#)
- [82] Paolo Petta, Catherine Pelachaud, and Roddy Cowie. *Emotion-Oriented Systems: The Humaine Handbook*. Springer Publishing Company, Incorporated, 2011. [1](#)
- [83] Rosalind W. Picard. *Affective Computing*. MIT Press, 1997. [1](#)
- [84] I. Poggi, C. Pelachaud, F. de Rosi, V. Carofiglio, and B. De Carolis. *Greta. A Believable Embodied Conversational Agent*, pages 3–25. Springer, 2005. [2](#)

- [85] Xingqun Qi, Chen Liu, Lincheng Li, Jie Hou, Haoran Xin, and Xin Yu. EmotionGesture: Audio-driven diverse emotional co-speech 3d gesture generation, 2023. [3](#)
- [86] Xingqun Qi, Chen Liu, Muyi Sun, Lincheng Li, Changjie Fan, and Xin Yu. Diverse 3D hand gesture prediction from body dynamics by bilateral hand disentanglement. In *Computer Vision and Pattern Recognition (CVPR)*, pages 4616–4626, 2023. [2](#)
- [87] Alec Radford, Jong Wook Kim, Chris Hallacy, Aditya Ramesh, Gabriel Goh, Sandhini Agarwal, Girish Sastry, Amanda Askell, Pamela Mishkin, Jack Clark, Gretchen Krueger, and Ilya Sutskever. Learning transferable visual models from natural language supervision. In *International Conference on Machine Learning (ICML)*, pages 8748–8763. PMLR, 2021. [3](#)
- [88] Robin Rombach, Andreas Blattmann, Dominik Lorenz, Patrick Esser, and Björn Ommer. High-resolution image synthesis with latent diffusion models. In *Computer Vision and Pattern Recognition (CVPR)*, pages 10674–10685, 2022. [4](#), [5](#)
- [89] Olaf Ronneberger, Philipp Fischer, and Thomas Brox. U-Net: Convolutional networks for biomedical image segmentation. In *Medical Image Computing and Computer-Assisted Intervention - MICCAI*, pages 234–241, 2015. [4](#)
- [90] Olga Russakovsky, Jia Deng, Hao Su, Jonathan Krause, Sanjeev Satheesh, Sean Ma, Zhiheng Huang, Andrej Karpathy, Aditya Khosla, Michael Bernstein, Alexander C. Berg, and Li Fei-Fei. ImageNet Large Scale Visual Recognition Challenge. *International Journal of Computer Vision (IJCV)*, 115(3):211–252, 2015. [13](#)
- [91] Tim Salzman, Marco Pavone, and Markus Ryll. Motron: Multimodal Probabilistic Human Motion Forecasting. In *Computer Vision and Pattern Recognition (CVPR)*, 2022. [2](#)
- [92] Klaus R Scherer. Vocal communication of emotion: A review of research paradigms. *Speech Communication*, 40(1-2):227–256, 2003. [1](#)
- [93] Maximilian Seitzer. pytorch-fid: FID Score for PyTorch. <https://github.com/mseitzer/pytorch-fid>, 2020. Version 0.3.0. [6](#)
- [94] Jiaming Song, Chenlin Meng, and Stefano Ermon. Denoising diffusion implicit models. In *International Conference on Learning Representations (ICLR)*, 2021. [5](#)
- [95] Kim Sung-Bin, Lee Hyun, Da Hye Hong, Suekyeong Nam, Janghoon Ju, and Tae-Hyun Oh. Laughtalk: Expressive 3d talking head generation with laughter. In *Winter Conference on Applications of Computer Vision (WACV)*, pages 6404–6413, 2024. [2](#)
- [96] Mingyang Sun†, Mengchen Zhao†, Yaqing Hou*, Minglei Li, Huang Xu, Songcen Xu, and Jianye Hao. Co-speech gesture synthesis by reinforcement learning with contrastive pre-trained rewards. In *Computer Vision and Pattern Recognition (CVPR)*, 2023. [2](#)
- [97] Marcus Thiébaux, Stacy Marsella, Andrew N. Marshall, and Marcelo Kallmann. SmartBody: behavior realization for embodied conversational agents. In *Adaptive Agents and Multi-Agent Systems (AAMAS)*, 2008. [2](#)
- [98] Hugo Touvron, Matthieu Cord, Matthijs Douze, Francisco Massa, Alexandre Sablayrolles, and Hervé Jégou. Training data-efficient image transformers & distillation through attention. In *International Conference on Machine Learning (ICML)*, pages 10347–10357, 2021. [4](#), [13](#), [14](#)
- [99] Jonathan Tseng, Rodrigo Castellon, and Karen Liu. Edge: Editable dance generation from music. In *Computer Vision and Pattern Recognition (CVPR)*, 2023. [2](#)
- [100] Ross Wightman. PyTorch image models (timm). <https://timm.fast.ai/>. Accessed: 2023-11-25. [15](#)
- [101] R. Williams. *The Animator’s Survival Kit: A Manual of Methods, Principles and Formulas for Classical, Computer, Games, Stop Motion and Internet Animators*. Farrar, Straus and Giroux, 2012. [2](#)
- [102] Jingyu Wu, Shi Chen, Shuyu Gan, Weijun Li, Changyuan Yang, and Lingyun Sun. Cultural self-adaptive multimodal gesture generation based on multiple culture gesture dataset. In *ACM International Conference on Multimedia (MM)*, page 3538–3549, 2023. [3](#)
- [103] Sicheng Yang, Zhiyong Wu, Minglei Li, Zhensong Zhang, Lei Hao, Weihong Bao, Ming Cheng, and Long Xiao. Diffusestylegesture: Stylized audio-driven co-speech gesture generation with diffusion models. In *International Joint Conference on Artificial Intelligence (IJCAI)*, 2023. [3](#), [6](#), [16](#), [17](#), [20](#)
- [104] Sicheng Yang, Zhiyong Wu, Minglei Li, Zhensong Zhang, Lei Hao, Weihong Bao, and Haolin Zhuang. Qpgesture: Quantization-based and phase-guided motion matching for natural speech-driven gesture generation. In *Computer Vision and Pattern Recognition (CVPR)*, pages 2321–2330, 2023. [2](#)
- [105] Payam Jome Yazdian, Mo Chen, and Angelica Lim. Gesture2vec: Clustering gestures using representation learning methods for co-speech gesture generation. In *International Conference on Intelligent Robots and Systems (IROS)*, pages 3100–3107, 2022. [2](#)
- [106] Hongwei Yi. Show github. <https://github.com/yhw-yhw/SHOW>, 2023. [6](#)
- [107] Hongwei Yi, Hualin Liang, Yifei Liu, Qiong Cao, Yandong Wen, Timo Bolkart, Dacheng Tao, and Michael J Black. Generating holistic 3d human motion from speech. In *Computer Vision and Pattern Recognition (CVPR)*, pages 469–480, 2023. [1](#), [2](#), [6](#), [7](#)
- [108] Li-Ping Yin, Yijun Wang, Tianyu He, Jinming Liu, Wei Zhao, Bohan Li, Xin Jin, and Jianxin Lin. Emog: Synthesizing emotive co-speech 3d gesture with diffusion model. *ArXiv*, abs/2306.11496, 2023. [3](#)
- [109] Youngwoo Yoon, Woo-Ri Ko, Minsu Jang, Jaeyeon Lee, Jaehong Kim, and Geehyuk Lee. Robots learn social skills: End-to-end learning of co-speech gesture generation for humanoid robots. In *International Conference on Robotics and Automation (ICRA)*, 2019. [6](#)
- [110] Youngwoo Yoon, Bok Cha, Joo-Haeng Lee, Minsu Jang, Jaeyeon Lee, Jaehong Kim, and Geehyuk Lee. Speech gesture generation from the trimodal context of text, audio, and speaker identity. *Transactions on Graphics (TOG)*, 39(6), 2020. [2](#), [6](#)
- [111] Youngwoo Yoon, Pieter Wolfert, Taras Kucherenko, Carla Viegas, Teodor Nikolov, Mihail Tsakov, and Gustav Eje

Henter. The geena challenge 2022: A large evaluation of data-driven co-speech gesture generation. In *International Conference on Multimodal Interaction*, 2022. 2

- [112] Ye Yuan and Kris M. Kitani. DLow: Diversifying latent flows for diverse human motion prediction. In *European Conference on Computer Vision (ECCV)*, 2020. 2
- [113] Yicheng Zhong, Huawei Wei, Peiji Yang, and Zhisheng Wang. Expclip: Bridging text and facial expressions via semantic alignment. In *AAAI Conference on Artificial Intelligence*, pages 7614–7622, 2024. 2
- [114] Yi Zhou, Connelly Barnes, Jingwan Lu, Jimei Yang, and Hao Li. On the continuity of rotation representations in neural networks. In *Computer Vision and Pattern Recognition (CVPR)*, pages 5745–5753, 2019. 3
- [115] Yi Zhou, Jingwan Lu, Connelly Barnes, Jimei Yang, Sitao Xiang, and Hao Li. Generative tweening: Long-term inbetweening of 3d human motions. *arXiv:2005.08891*, 2020. 2
- [116] Lingting Zhu, Xian Liu, Xuanyu Liu, Rui Qian, Ziwei Liu, and Lequan Yu. Taming diffusion models for audio-driven co-speech gesture generation. In *Computer Vision and Pattern Recognition (CVPR)*, pages 10544–10553, 2023. 2, 8, 16

APPENDIX

This supplementary material summarizes the video content in Appendix A and provides additional technical details of the speech disentangled model and the gesture generation model in Appendix B and Appendix C, respectively. We provide details about motion extractor model in Appendix D, discussions on the gesture emotion and semantics in Appendix E, details on the data preparation process in Appendix F, a review of state of the art methods in Appendix G, and additional information about the perceptual study in Appendix H.

A. Supplementary Video

The supplementary video shows the generated gestures. Specifically, it provides:

1. Gesture generations on various emotional audios,
2. Gesture emotion and style editing results,
3. Comparisons with state of the art mesh-based and skeleton-based gesture generation methods,
4. Ablation comparisons of the different components of our approach,
5. Gestures showing the diversity in the generations, and
6. Gestures generated from an in-the-wild audio sequence.

B. Speech Disentanglement Model

We explain the overall architecture in Appendix B.1 and the encoder–transformer architecture in Appendix B.2. We demonstrate the reconstruction mechanism to enforce dis-

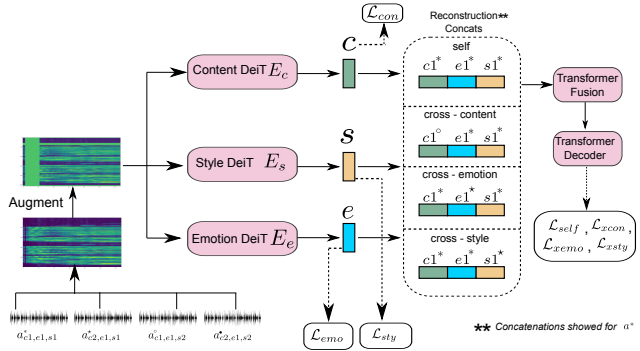


Figure A.1. **Speech disentanglement model.** An input filterbank is given to the three encoders, producing three disentangled latents, which are decoded into a reconstructed filterbank. We here show disentanglement reconstruction for one audio only, please refer Appendix B.3 for its detailed explanation.

entanglement in Appendix B.3. Finally, we explain the training procedure and loss terms in Appendix B.4.

B.1. Architecture

We illustrate speech disentanglement model architecture in Fig. A.1. The training is conducted over audio of the same utterances spoken under different emotions or spoken by different speakers. Our model consists of three transformer encoders, a transformer fusion, and a transformer decoder. The input filterbank is simultaneously passed through content E_c , style E_s , and emotion E_e transformer encoders, producing three disentangled latents: content c , style s , and emotion e . The fusion and decoder are transformer-based layers. The transformer–fusion creates a single embedding by applying cross attention on the input triplet embeddings (c, e, s) . Finally, the transformer–decoder reconstructs the original filter bank from the compressed single latent embedding produced by the transformer fusion.

B.2. Encoder Transformers

Similar to [25–28, 31, 74] we employ transfer learning of vision task to our audio task by using pretrained weights of DeiT [98] (88M params) transformer that is fine-tuned on 384x384 images from ImageNet-1k [90]. We use a pretrained DeiT encoder as a component of each of the encoders, as illustrated in Fig. A.3. We linearly embed patches to features embedding of size 768 and feed them into DeiT along with trainable positional embedding of same size (768). We append class token [CLS] and distillation token [DIST] obtained from DeiT at the beginning of each filter bank sequence. We then average the 3-channel inputs of DeiT to obtain a single filterbank channel input. Finally, we use the output of the last DeiT encoder layer and project to 1D latent vector of 256 dimensions each, as our con-

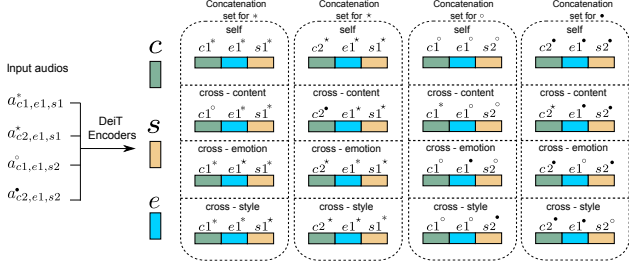


Figure A.2. **Reconstruction concatenations for training forward pass.** We obtain disentangled content, emotion, and style latents from the transformer encoders. (*Self*) concatenation of triplet latent vectors is used to decode back into the original filterbank. To enforce the content disentanglement, we swap content latent vectors (*cross-content*) between given different-subjects audio pair with same utterances. Whereas to enforce style and emotion disentanglement, we swap style (*cross-style*) and emotion (*cross-emotion*) latent vectors between given same-subject audio pairs with same emotion categorical label. We repeat the procedure for quadruples of audio $\{a^*, a^*, a^\circ, a^\bullet\}$ input in each forward pass.

content, emotion, and style latents. We average the [CLS] and [DIST] tokens from DeiT and use it for audio emotion as well as audio style classification tasks for 8 and 30 category labels respectively.

B.3. Reconstruction Concatenations

Fig. A.2 demonstrates a detailed information of the cross-reconstruction mechanism to enforce the audio content, emotion, and style disentanglement. Each audio in the quadruple is encoded and decoded to produce the reconstructed audio filterbank. To enforce content disentanglement, we swap the content latent vectors between different-subject same-emotion audio pairs with same utterances. Similarly, we swap emotion and style latents using audio pairs from the same subject. Specifically, we swap emotion latent vector and style latent vector between same-subject same-emotion audio pairs with different utterances. The procedure is repeated for each audio in the audio quadruples.

B.4. Training and Losses

We train the speech disentanglement model on 10s-audio segments of the BEAT dataset, which provides the GT labels for emotion and subject categorical labels. We split the audio data across actors during train, validation, and test step. During training, one sample is formed by a quadruple of different audios ($a_1 = a_{c_1, e_1, s_1}, a_2 = a_{c_2, e_1, s_1}, a_3 = a_{c_1, e_1, s_2}, a_4 = a_{c_2, e_1, s_2}$), with two different contents c_1, c_2 (i.e., two different scripts), two different styles s_1, s_2 (spoken by two different subjects) and the same emotion e_1 . To ensure, content, style, and emotion disentanglement, we employ a multitude of training losses. The

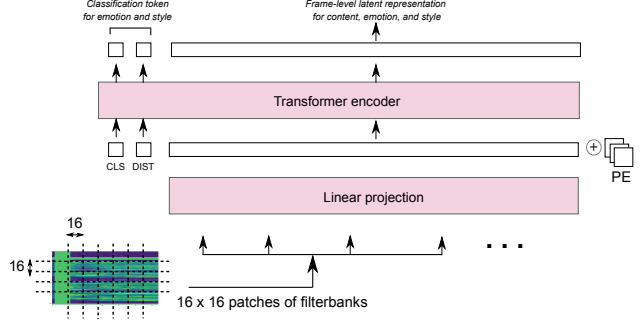


Figure A.3. **Speech encoder transformer.** We have used encoder architecture based on Touvron et al. [98]. We use this architecture as content, emotion, and style encoders in the speech disentanglement model. Following Gong et al. [25, 27], we use 10s augmented speech filterbank and split into fixed 1209 patches of 16 x 16 each, having 6 units overlap in frequency and time domain. The filterbank is passed through a linear projection layer and a learnable positional embedding (PE) is added to it.

self-reconstruction loss \mathcal{L}_{self} ensures that the style, emotion, and content latents extracted from the same audio can be decoded into the original inputs:

$$\mathcal{L}_{self} = \sum_{k=1}^4 \|D(E_c(a_k), E_s(a_k), E_e(a_k)) - a_k\|_1$$

The content loss \mathcal{L}_{con} ensures that two content latents extracted from two different audios with the same content c_k but two different styles s_i, s_j match:

$$\mathcal{L}_{con} = \sum_{k=1}^2 \|E_c(a_k) - E_c(a_{k+2})\|_1$$

We also employ the emotion classification loss \mathcal{L}_{emo} to ensure that the encoded emotion latents carry the emotion information. This is ensured by projecting them with a linear projection head into a classification vector and then computing emotion classification cross entropy loss. We use the same procedure to employ the style classification loss \mathcal{L}_{sty} :

$$\mathcal{L}_{emo} = - \sum_{1 \leq l_e \leq n_e} y_{l_e} \log(p_{l_e}),$$

$$\mathcal{L}_{sty} = - \sum_{1 \leq l_s \leq n_s} y_{l_s} \log(p_{l_s}),$$

with $n_e = 8$ and $n_s = 30$ denoting the number of emotion classes and training subjects respectively.

Finally, we employ the cross-reconstruction losses for emotion, style, and content. This loss ensures that we can combine any three style, content, and emotion latents and decode them into a valid reconstruction. As shown

in Fig. A.1 and Fig. A.2, this is a three part cross reconstruction process. In this process, we extract content $E_c(a_*)$, emotion $E_e(a_*)$, and style $E_s(a_*)$ latents of all four different audios. Given two input audios of the different contents c_i and c_j , with the same speaker, and the same emotion, we swap the emotion latents between the audio pair, and decode the two audios back. Since the emotion class is constant within a quadruple, the emotion cross-reconstruction should be equal to the original audio. Similarly, we cross-reconstruct an input audio with two style latents of the same person, but of different sequence. Enforced by:

$$\mathcal{L}_{xemo} = \sum_{k=1}^4 D(E_c(a_k), E_s(a_k), E_e(a_{j(k)})) - a_k,$$

$$\mathcal{L}_{xsty} = \sum_{k=1}^4 D(E_c(a_k), E_s(a_{j(k)}), E_e(a_k)) - a_k,$$

where $j(k) = [(6 - k) \bmod 4] + 1$.

Given two input audios of the same contents, different speakers s_i and s_j , and same emotion, we swap the content latents between the audio pair, and decode the two audios back. Since the utterances being spoken are the same and we keep the original style and emotion constant, the cross reconstruction for the swapped content should be equal to original audio. This is enforced by:

Table A.1. **Audio emotion and style disentanglement ablation.** We show scores for Emotion Accuracy (EA), Style Accuracy (SA), Emotion F1 Score (EF1), and Style F1 Score (SF1) in our speech disentanglement model and ablation experiments. Although there are slight differences, our model effectively captures the complex relationships between emotion and style by disentangling three latent vectors simultaneously. The best scores are highlighted in green and second best in blue.

Method	EA (%) \uparrow	EF1 \uparrow	SA (%) \uparrow	SF1 \uparrow
Ours	91.531	0.914	96.060	0.960
Emo-disentangle	91.966	0.918	—	—
Sty-disentangle	—	—	96.095	0.961

Table A.2. **Audio latent component factorization ablation.** Self and cross-reconstruction errors show comparable performance, suggesting that individual latents from different audio sources can be effectively combined to yield valid outputs. The best scores are highlighted in green and second best in blue.

Method	Self \downarrow	XCon \downarrow	XEmo \downarrow	XSty \downarrow
Ours	.3739	.3740	.3816	.3815
Emo-disentangle	.3793	.3792	.3905	—
Sty-disentangle	.3769	.3770	—	.3887

$$\mathcal{L}_{xcon} = \sum_{k=1}^4 D(E_c(a_{j(k)}), E_s(a_k), E_e(a_k)) - a_k$$

where $j(k) = [(1 + k) \bmod 4] + 1$.

The combined audio loss is given as:

$$\mathcal{L}_{dis} = \mathcal{L}_{xcon} + \mathcal{L}_{xemo} + \mathcal{L}_{xsty} + \mathcal{L}_{self} + \mathcal{L}_{emo} + \mathcal{L}_{con} + \mathcal{L}_{sty}$$

Once trained, the speech disentanglement model produces three disentangled latents for content, style and emotion. These latents serve as the input to our diffusion model.

B.5. Implementation Details

The encoder transformer DeiT (88M parameters) that is finetuned on 384x384 images from ImageNet-1k is obtained from PyTorch image models (timm) [100]. The content, emotion, and style latent vectors are of 256 dimension. The transformer-fusion includes 2 layers and 4 heads. The transformer-decoder includes 4 heads and 4 layers. The input dimension of fusion block is 768 to accommodate three content, emotion, and style latent codes. Each 2D filterbank is of 1024 x 128, where 128 represents the number of mel-frequency bins.

B.6. Ablation Experiments

We conduct two ablation studies with the speech disentanglement model. One to only disentangle emotion from content (dropping \mathcal{L}_{sty} , \mathcal{L}_{xsty}). The other to only disentangle only style from content (dropping \mathcal{L}_{emo} , \mathcal{L}_{xemo}). Tab. A.1 shows the accuracy and F1 scores for emotion and style latent vectors. The Emotion Accuracy (EA), Style Accuracy (SA), Emotion F1 Score (EF1), and Style F1 Score (SF1) in our speech disentanglement model exhibit only marginal differences compared to the results obtained in the ablation experiments. We report the test set self- and cross-reconstruction errors in Tab. A.2. The cross-reconstruction errors are comparable to self-reconstruction errors which indicates that the individual latents from different audios can be combined to produce valid outputs. This holds for the main model and also the ablated models. However, the ablated models are not able to factor the audio into all three components due to the dropped loss terms. We observe the robust performance of our audio model, by accounting for the complex interplay between emotion and style. By concurrently disentangling three latent vectors, our approach effectively captures the intricate relationships in the audio data, allowing to jointly model and distinguish both emotion and style factors.

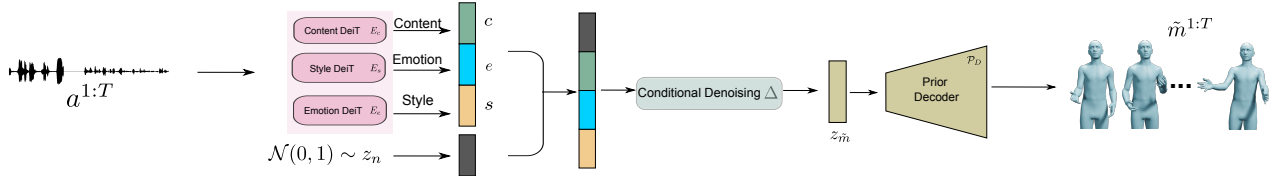


Figure A.4. **Inference.** We sample z_n and employ the three conditioning latents from a test-time audio c, e, s . We iteratively apply Δ to generate the fully denoised $z_{\tilde{m}}$ which is decoded by \mathcal{P}_D into the final motion $\tilde{m}^{1:T}$.

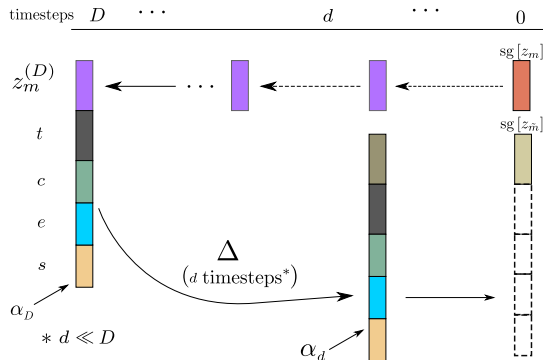


Figure A.5. **Conditional latent diffusion.** In the diffusion process (right to left) we obtain a noisy motion latent, whereas in the denoising process (left to right) we obtain a conditioned denoised motion latent.

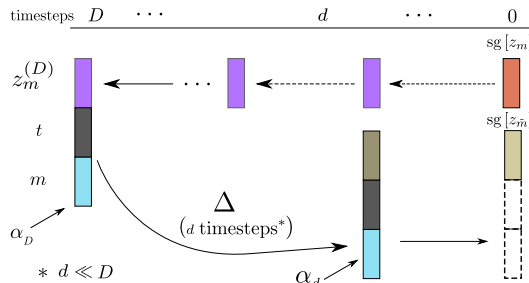


Figure A.6. **Ablation conditional latent diffusion.** In the denoising process (left to right) of the ablation model, we obtain a denoised motion latent that is conditioned on a compressed non-disentangled latent vector m instead of three disentangled latents that are used in the final model.

C. Gesture Generation Model

C.1. Motion Prior And Latent Denoiser

In this section we include detailed illustrations of the motion prior and latent denoiser. Fig. A.4 illustrates the inference process employed by our model. Fig. A.5 illustrates the forward diffusion and the reverse audio-conditioned denoising process, operating at the latent space. Finally, A.7 shows the diagram of the architecture of the motion prior.

C.2. Methods Trained on Coarse Skeletal Data

We compare AMUSE with methods trained on coarse skeletal data. We choose DSG [103], CaMN [58], Zhu et al. [116] and MoGlow [4] as recent gesture generation models using audio input. AMUSE produces more synchronized gestures and better represents the underlying audio emotion compared to the state of the art methods trained on skeletal data, as shown in our supplementary video. Additionally, these methods are not trained to output 3D meshes. We observe uncanny poses and self-penetrations as shown in Fig. A.8. In our video, we provide additional comparison with these skeleton based methods in both formats, the original predictions of those models and 3D meshes which are created via Inverse Kinematics (IK). We exclude the conversion to 3D mesh for Zhu et al. [116] because the output skeleton format is incompatible with SMPL-X topology.

C.3. Ablation Experiments

Without speech disentanglement model. This subsection illustrates the difference between the final AMUSE model and the ablation of AMUSE w/o audio disentanglement. AMUSE w/o audio disentanglement uses 8 linear-layered auto-encoder that operates directly on raw audio MFCC features to produce single latent vector m . Since AMUSE w/o audio disentanglement does not operate over the three disentangled latents of content, emotion, and style but instead only one non-disentangled latent m , the latent diffusion process also only takes one latent on the input m as shown in Fig. A.6. By design, this model lacks the gesture editing capabilities.

Without motion prior. We employ our latent denoiser only in this ablation model. We completely removed the motion prior component and replace it with a linear projection head. The ablation model without motion prior is not able to converge and produces mostly static motions (refer to the supplementary video). This signifies the importance of having a motion prior component in our AMUSE architecture.

Quantitative evaluation of ablation experiments. Following the procedure described in the Sec. 5.1, we report quantitative evaluation scores in Tab. A.3, comparing AMUSE with the ablation models and GT. The version w/o speech disentanglement model produces lower-quality gestures and lacks editing capabilities compared to the complete model. This is because it lacks a component for sep-

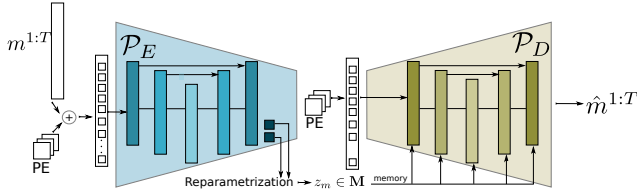


Figure A.7. **Motion prior network.** The motion prior is VAE encoder-decoder architecture inspired from Chen et al. [15]. Both encoder and decoder follow a U-Net like structure with skip connections between transformer blocks. The learnable positional embeddings (PE) are injected into each multi-head attention layer.

arating emotion, content and style in the audio. The scores for the ablation models without motion prior are the lowest, indicating that this model did not converge successfully. Additionally, in Tab. A.4 we report improved FGD and Div scores when the motion prior and diffusion model are trained jointly compared to when trained separately, indicating that joint training yields superior results. Furthermore, we conduct additional ablation experiments with and without alignment losses (\mathcal{L}_{align} , \mathcal{L}_{Valign}). Including alignment losses results in a GA of 46.79%, whereas without them, the GA drops to 30.89%, demonstrating the alignment losses effectiveness. Moreover, we compute the average jerk of the left and right hands for motion sequences belonging to the same audio of [103], ours, and GT, reporting it in m/s^3 as 1.18, 1.10, and 0.065, respectively. This signifies that the GT motion is the most steady, whereas ours is

Table A.3. **Ablation of AMUSE components.** The model without audio disentanglement produces lower-quality gestures and lacks editing capabilities. The model without motion prior perform poorly due to convergence issues. Among the methods being compared, we highlight the best scores in green and second best in blue.

Method	SRGR \uparrow	BA \uparrow	FGD \downarrow	Div \rightarrow	GA \uparrow
GT	—	0.83	—	27.83	64.04
Ours	0.36	0.81	388.63	25.06	46.76
Ours-No-Prior	0.25	0.20	987.90	13.41	15.42
Ours-No-Audio-Model	0.31	0.78	633.27	21.08	26.88

^a GA is average of all 8 emotions.

Table A.4. **Ablation of AMUSE training.** We observe improved FGD and Div scores when the motion prior and diffusion model are jointly trained, highlighting superior performance compared to separate training methods. We highlight the best scores in green and second best in blue.

Method	FGD \downarrow	Div \rightarrow
Ours	388.63	25.06
Ours-Disjoint	362.33	24.49

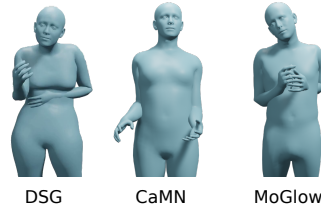


Figure A.8. **Coarse skeleton-based methods.** Here we compare DSG [103], CaMN [58], and MoGlow [4]. Unlike SMPL-X-based models, these are trained using different skeletal hierarchies without volumetric 3D shapes. Retargeting them onto the SMPL-X skeleton with IK causes uncanny poses and self-penetration.

slightly smoother over time compared to [103].

D. Motion Feature Extractor Model

We employ the motion extractor model M for computing all quantitative evaluation metrics. Our motion extractor encoder model design is inspired by Petrovich et al. [80], in an autoencoder setting (i.e., without a probabilistic variational component). We append a CLS token at the beginning of the motion sequence and supervise with a cross-entropy emotion classification objective \mathcal{L}_{Memo} applied to the output CLS token. We train the motion extractor model on the BEAT training data. Once trained, we use the latent space features to compute evaluation metrics as described in the Sec. 5.1.

$$\mathcal{L}_{Memo} = - \sum_{1 \leq l_e \leq n_e} y_{l_e} \log(p_{l_e})$$

with $n_e = 8$ denotes the number of emotion classes.

E. Gesture Emotions And Semantics

We quantitatively evaluate our method using metrics SRGR, beat align, FGD, diversity, and gesture emotion accuracy. Leveraging the latent space features from the motion extractor model M , we compute SRGR and gesture emotion accuracy. Additionally, we directly utilize the generated motion sequence to calculate the beat align score.

Semantic-Relevant Gesture Recall (SRGR). In the SRGR metric score, similar to Liu et al. [58], we use ground truth semantic score as weight for the Probability of Correct Keypoint (PCK) between the generated gestures and ground truth gestures, where PCK is the number of joints successfully recalled for a given threshold δ . Following the approach suggested by BEAT authors:

$$SRGR = \lambda \sum \frac{1}{T \times J} \sum_{t=1}^T \sum_{j=1}^J \mathbf{1} \left[\left\| p_t^j - \hat{p}_t^j \right\|_2 < \delta \right]$$

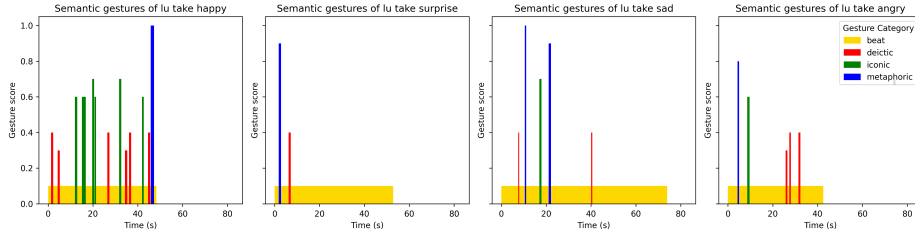


Figure A.9. **Emotional gesture variation.** Semantic scores for various emotions within the same subject shows how the subject expresses gestures differently for each emotion. This reflects the subject’s interpersonal style specific to each emotion.

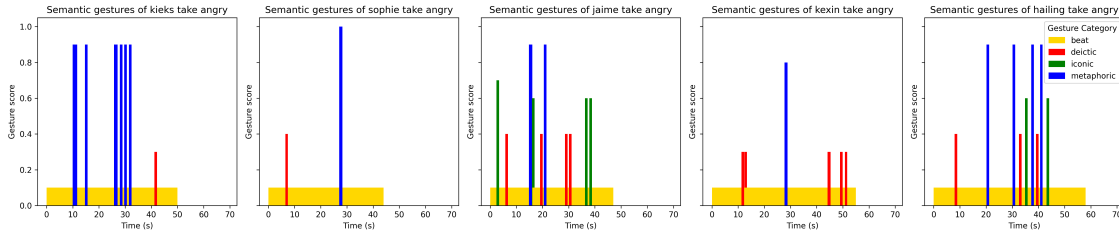


Figure A.10. **Emotional gesture individuality.** Semantic scores across various subjects for the same emotion reveal how different subjects express gestures uniquely for identical utterances within same emotion. There is variability in expressiveness, with some subjects being more expressive (eg. Jamie, Hailing) than the others (eg. Sophie, Kexin).

where $\mathbf{1}$ is the indicator function, T , J are the set of frames and number of joints, we use SRGR to measure how well our model recalls gestures in the relevant clip. This metric reflects human perception of valid gesture diversity. The metric is computed based on the scores assigned by 118 annotators from Amazon Mechanical Turk (AMT), who evaluated the semantic relevance on a continuous scale of 0-1. The scores are provided for four gesture types: beat (*rhythmic movements*), iconic (*representative movements*), deictic (*indicative or pointing movements*), and metaphoric (*symbolic or figurative movements*). SRGR metric needs GT semantic scores for computation.

Ground-truth semantic scores. We obtain the ground-truth semantic score, provided by the BEAT authors, for computing the SRGR. In Fig. A.9, we present semantic scores for the same subject across various emotions, while Fig. A.10 illustrates semantic scores for all subjects expressing the same emotion. This allows us to observe how subjects gesture differently with different emotions and how different subjects gesture for the same emotion. While we acknowledge the high-quality dataset introduced by the BEAT authors, our model has the potential to deliver even better results and improved expressivity with an enhanced dataset quality.

Beat alignment. Following Li et al. [53], we compute the beat align score. To compute the beat alignment score, we use six joints: left wrist, left elbow, left shoulder, right wrist, right elbow, and right shoulder, similar to Liu et al. [58]. We measure the synchronization between the generated 3D motion and the input speech by calculating the beat align

score. This score gauges the average distance between each kinematic beat and its nearest speech audio beat, following a unidirectional approach – recognizing that gesture motion may not align with every speech audio beat. AMUSE achieves the highest beat align score in correlating speech audio and gestures compared to the other methods.

Gesture emotion accuracy. Gestural emotions are complex, influenced by internal states of subject, social signals, and their perception vary significantly across individuals with diverse cultural backgrounds. AMUSE is designed to capture perceived gestural emotions. While we demonstrate AMUSE with a gesture emotion recognition accuracy of 46.76% and AMUSE-Edit with 34.18%, outperforming other state of the art methods, it is important to note that recognizing emotion from gestures remains a challenging task in computer vision. We observe the gesture emotion accuracy for the GT sequence is 64.04%. There is still ample room for improvement in addressing this complex problem. Additionally, in Fig. A.12, we present the confusion matrix for ground truth (GT) emotion predictions on the left and reconstructions (gestures generated using the original style, emotion, and content latents of a given audio) on the right. We observe a robust correlation between the predictions on GT and the reconstructions for all eight emotions. Additionally, we conducted experiments on gesture edits by swapping emotion latents from one audio with those from another audio of the same subject but with a different utterance. In Fig. A.11, we showcase two exemplars, transforming from *Happy to rest* and *Surprise to rest*. Given the diversity of eight emotions, gestural edits offer numerous pos-

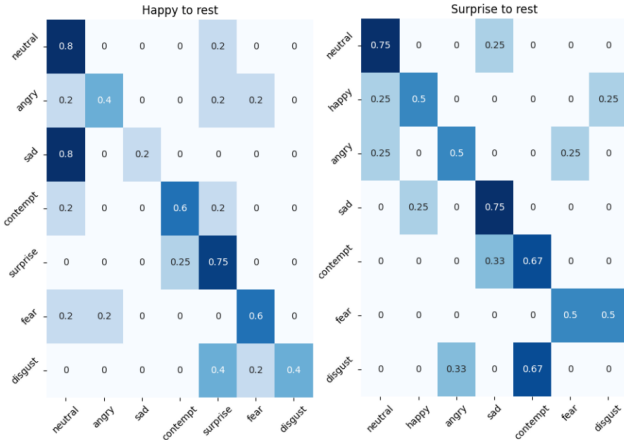


Figure A.11. **Emotion edit confusion matrix, displaying transitions from Happy (left) and Surprise (right) emotions to others.** X-axis is for predictions and Y-axis is for ground truth.

sibilities, rendering this a broad and challenging problem. Although Fig. A.11 displays promising results for emotion label predictions with clear diagonal pattern of the confusion matrix, we acknowledge the inherent difficulty in solving this problem.

F. Data Preparation

In this section, we describe the processing and alignment of different modalities, and the BEAT [58] data subsets employed to train the different models of our framework. We do not use the entirety of the BEAT dataset to train AMUSE. BEAT contains 30 speakers. We filter out subjects with little expressivity in their motion through visual inspection of GT, leaving us with 22 subjects. Furthermore, BEAT has a subset that all the subjects speak the same sentences in the same emotions. The rest of the dataset contains unique sentences which are spoken only by one speaker and not the others. We filter out all of these unique sentences. What remains is a subset of 16 sentences (2 per emotion, for 8 emotions), spoken by every subject. This is critical since the training of the speech disentanglement module requires

Table A.5. **Perceptual study.** We demonstrate aggregate scores of our perceptual study, and we disregard indifferent scores. The *ours* and *others* are sum of % preference for (strongly ours and weakly ours) and (strongly other and weakly other) respectively. Only the best scores are highlighted in **green**.

Criteria → Method ↓	Emotion		Synchronization	
	Ours	Others	Ours	Others
GT	38	51	35	52
TalkSHOW-BEAT	46	39	62	27
TalkSHOW	54	34	65	28
Habibie et al.	48	42	66	28

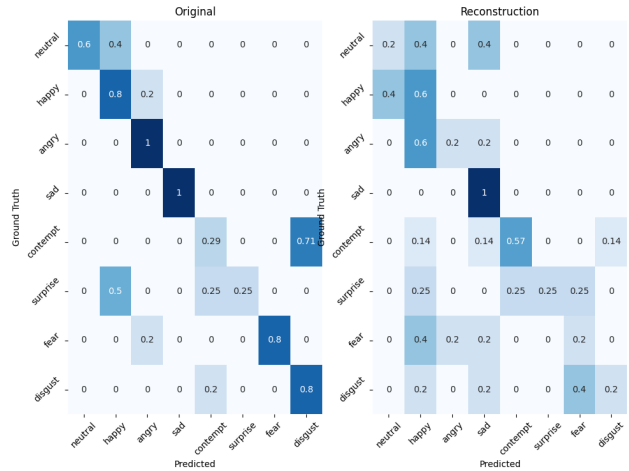


Figure A.12. **Confusion matrix comparing gestures from the ground truth (GT) and regenerated emotion predictions.**

perfect temporal correspondence between the audios of the same sentences. Except where explicitly stated otherwise, we have used this subset and split it into train, validation, and test sets. This subset is 5.71 hours long. We use the same data to train our speech disentanglement model. Further, we train our motion prior network ($\mathcal{P}_E, \mathcal{P}_D$) with the extracted SMPL-X motions of the same subsets. Finally, the denoiser, Δ , and feature extractor used for evaluation, M , are trained on the same subset and splits.

G. Review of State of the Art Methods

Data selection and input formats. To train AMUSE effectively, we require data in the form of 3D point clouds rather than coarse BVH skeletons. Additionally, training requires common utterances from multiple subjects expressing various emotions for audio disentanglement. Many available gesture datasets, including [21, 75], come in various motion capture skeleton formats with different underlying kinematic hierarchies that are incompatible with our conversion procedure to obtain SMPL-X meshes and do not meet the requirement of speech common utterances. In contrast, for the BEAT dataset, we obtained the initial data in the form of 3D point clouds from the dataset authors. We use Mosh++ [61, 65] to extract SMPL-X pose and shape parameters, along with global translation and orientation, from the 3D point cloud. This data was then used to train AMUSE.

SOTA methods and modifications. Given our primary objective is to generate 3D emotional gestures from audio input, we mainly compare state-of-the-art methods that use audio input alone and output a 3D mesh. We exclude methods that incorporate additional inputs, such as arbitrary lengths of target motion style, as they deviate from our main objective, for example, Ghorbani et al. [21]. Other recent

works [5, 7] have proposed methods for generating gestures from speech. However, making direct comparisons is difficult as the code for their approaches is not publicly available. We retrained Henter et al. [37] using publicly available code and instructions, due to the unavailability of a pretrained model. In our comparison, we used publicly available DSG [103] model that was trained on the BEAT dataset of coarse skeletal format. We also made modifications to the TalkSHOW code, incorporating emotion labels as input, and retrained it on the same data used for training our model. The emotion categorical labels were injected inline with existing subject labels using one-hot vectors. AMUSE outperforms both DSG and TalkSHOW-BEAT as well as other SOTA methods in all comparisons.

H. Additional Perceptual Study Details

Here we describe additional details of the AMT study reported in the Sec. 5.3. We show aggregate preference scores in Tab. A.5. AMUSE outperforms all methods compared against in both criteria - synchronization with the speech and the appropriateness with respect to the specified emotion. In contrast, Ground Truth (GT) consistently outperforms AMUSE in both tasks. This outcome emphasizes the complexity of the problem, where achieving synchrony with speech and meeting specified emotional appropriateness remain challenging objectives.

Data. We randomly select three videos per emotion from the BEAT dataset for our perceptual study. We only use sequence that were not part of training or validation set. Due to high number of subjects, we limit the input audios data to only two subjects.

The template layout. Fig. A.13 depicts the design template that the participants were shown. The left-right position of our method and the competing methods was randomized to factor out any biases that participants may have for one side or the other.

Catch trials. Each participant was also shown three catch trials, where a GT video was shown alongside a broken motion filled with artifacts. Participants that did not select weak or strong preference for the GT video in any of the catch trials were labeled as uncooperative or inattentive and were not considered in the analysis. We selected 22, 20, 23, and 25 participants for TalkSHOW-BEAT, TalkSHOW, Habibie et al., and GT, respectively, from a total of 25 Amazon Mechanical Turk workers.

Decide which video has better gesticulation

In this task you are presented with two videos of animated virtual characters. Their gestures are generated based on the same audio.

Both videos have sound, please listen to them!

You will be asked to select your preference between the two videos according to two different criteria:

1. Which video has better synchronization of gestures and speech rhythm?
(Speech rhythm is the arrangement of spoken words alternating stressed and unstressed elements. You have to decide which animated character has gestures that are better aligned with the speech rhythm.)

2. In which video do the gestures better represent the emotion?
(The emotion is specified in the question below for each video. You have to decide which animated character has gestures that better represent the given emotion.)

Please focus on gestures alone and NOT on the facial expression of the characters - the face is static (not animated) and is not the point of this study.

Choose your preference on the scale from left to right, where the leftmost answer means strong preference for the video A, and the rightmost answer means strong preference for the video B, and the middle radio button means no preference.

Please press play in order to start the videos. You need to watch and listen both videos at least once to be able to answer.

video A



video A

video B



video B

1. Which video has better synchronization of gestures and speech rhythm?

strong preference for video A
 weak preference for video A
 equally preferred
 weak preference for video B
 strong preference for video B

2. The characters are feeling the following emotion: **disgust. Which of the two characters gestures this emotion better?**

strong preference for video A
 weak preference for video A
 equally preferred
 weak preference for video B
 strong preference for video B

To proceed, you must select an answer to all questions!

Next video

30 videos left

SUBMIT

Figure A.13. **The layout of the perceptual study.** The participant is shown two videos and asked to enter their preference according to two criteria - synchronization with the speech and the appropriateness with respect to the specified emotion.